frontiers in Earth Science

REVIEW
published: 11 March 2019
doi: 10.3389/feart.2019.00017

Hydrothermal Production of H_2 and Magnetite From Steel Slags: A Geo-Inspired Approach Based on Olivine Serpentinization

*Fabrice Brunet**

Univ. Grenoble Alpes, Univ. Savoie Mont Blanc, CNRS, IRD, IFSTTAR, ISTerre, Grenoble, France

The interaction between ultramafic rocks and hot seawater at slow-spreading mid-oceanic ridges triggers hydrothermal redox reactions which are known to produce magnetite and H_2 under appropriate pressure and temperature conditions. Steel slags share some common properties with ultramafic rocks. They are composed of anhydrous and refractory minerals formed at temperatures exceeding 1,200°C and they contain ferrous iron in comparable amounts. Consequently, when submitted to hydrothermal conditions both types of materials, natural and anthropogenic, are prone to form magnetite and H_2 according to the simplified redox reaction:

$3[FeO] + H_2O => Fe_3O_4 + H_2$ (1)

where [FeO] is the ferrous iron component of the corresponding material that can be present under different mineralogical forms. Since H_2 and magnetite are two valuable products for applications in new technologies, the hydrothermal treatment of steel slags can be seen as a way to valorize a byproduct of the steel industry, a few tenths of a billion tons of which are produced yearly. The hydrothermal behavior of steel slags which arise from basic oxygen furnace (BOF) operations and that of olivine $(Mg,Fe)_2SiO_4$, the main mineral constituent of abyssal peridotites, are described here based on data from the literature. The thermochemical characteristics of Reaction 1 are reviewed for both types of materials in the perspective of optimizing a process that would valorize BOF steel slags for the production of nanomagnetite (and high-purity H_2). In particular, the kinetics effect of temperature, pH and solution-to-solid mass ratio on the hydrothermal oxidation of wüstite (FeO), considered here as an analog of the ferrous-iron component of steel slags, are modeled. The possible role of additives (impurity) on the hydrothermal oxidation of wüstite through the catalysis of the water-splitting reaction is discussed. Finally, the lack of kinetics constraints on nanomagnetite growth under hydrothermal conditions in a wide range of pH is identified as a major gap in the understanding of two important issues: (1) the catalysis of abiotic molecules in the course of serpentinization reactions, and (2) the tailoring of the size of the magnetite produced by hydrothermal treatment of BOF steel slags.

Keywords: H_2, magnetite, steel slags, geo-inspiration, serpentinization, olivine, water splitting

OPEN ACCESS

Edited by:
Jean-Philippe Perrillat, Claude Bernard University Lyon 1, France

Reviewed by:
Hannah Miller, Colorado State University, United States
Martin Charles Wilding, Sheffield Hallam University, United Kingdom

***Correspondence:**
Fabrice Brunet
fabrice.brunet@univ-grenoble-alpes.fr

Specialty section:
This article was submitted to Earth and Planetary Materials, a section of the journal Frontiers in Earth Science

Received: *01 November 2018*
Accepted: *30 January 2019*
Published: *11 March 2019*

Citation:
Brunet F (2019) Hydrothermal Production of H_2 and Magnetite From Steel Slags: A Geo-Inspired Approach Based on Olivine Serpentinization. Front. Earth Sci. 7:17. doi: 10.3389/feart.2019.00017

INTRODUCTION

The notion of biomimetics which encompasses designs, adaptation or derivation which are biologically inspired (Bhushan, 2009), is so popular in the scientific community that biomimetics is a recognized field with dedicated journals. Comparatively, geo-inspiration which is linked to geological processes has received much less attention. The present publication describes one example of a geo-inspired approach related to the valorization of iron-bearing wastes and byproducts from the steel industry.

The source of inspiration lies in hydrothermal reactions which take place at slow-spreading ridges where seafloor spreading is partly accounted for by large-scale detachment faults that bring lithospheric mantle peridotites to shallow levels (Cannat et al., 2006). The interaction between seawater and these partly exhumed ultramafic rocks triggers mineralogical reactions that liberate thermal and chemical energy by means of highly exothermic reactions and by the production of H_2, a gas of high specific energy, respectively (**Figure 1**). Both heat release and H_2 production result from the reactions between seawater and refractory Fe^{2+}-bearing silicates, olivine and orthopyroxene. Hydrous minerals of the serpentine group are formed along with magnetite, Fe_3O_4. Ferrous iron is partly oxidized in these hydrothermal reactions and H_2 is thus produced. Magnetite is a mineral which displays remarkable physical properties of density, magnetism, heat capacity and thermal conductivity (Blaney, 2007; Grosu et al., 2017), all of which make it a valuable material for many technical and high-tech applications.

As upper-mantle rocks, steel slags result from a high-temperature process, operated under dry conditions. They are produced at ca. 1,600°C in a converter (BOF) or in an electrical arc (EAF) furnace (**Figure 1**). Steel-making slags are also highly reactive with water according to exothermic hydration reactions (e.g., Juckes, 2003; Wang and Yan, 2010). Furthermore, BOF and EAF slags show a ferrous iron content that compares well with that of peridotites, although iron is mostly hosted by magnesio-wüstite instead of silicate minerals. Inspired by the hydrothermal reactions occurring at slow-spreading ridges, Malvoisin et al. (2013) submitted BOF slags to a hydrothermal treatment and showed that H_2 and magnetite were produced according to a process that can be defined as geo-inspired. Owing to the economic value of both H_2 and magnetite, the work by Malvoisin et al. (2013) has been further complemented by experimental studies to better characterize the paths and kinetics of reactions that lead to the formation of magnetite and H_2 from BOF or BOF-like starting materials (Crouzet et al., 2017a,b,c). This experimental work on slags adds up with a large number of experimental geochemistry studies on the Fe-bearing forsterite behavior under hydrothermal conditions. The purpose of the present contribution is to review the thermochemical characteristics of the two types of Fe^{2+}-bearing systems, natural and anthropogenic, when they are submitted to hydrothermal conditions. The leading idea is to see how the thermochemical knowledge gained on hydrothermal magnetite and H_2 production from both geological and slag materials can each shed light on the other. In particular, the effect of temperature, pH, water-to-solid mass ratio and impurities on reaction kinetics and on the characteristics of the reaction products will be examined for the two systems.

MAGNETITE AND H_2 PRODUCTION BY RECYCLING FERROUS WASTES: MOTIVATION AND GEO-INSPIRED APPROACH

A parallel can be made between the notions of geo-inspiration and biomimetics, the latter being by far more popular. Vincent et al. (2006) defined biomimetics as "the practical use of mechanisms and functions of biological science in engineering, design, chemistry, electronics, and so on." The authors recall that people have looked to nature for inspiration for more than 3,000 years. This inspiration seems, however, to have mostly concerned biology with the main challenge of transferring a concept or a mechanism from living to non-living systems as pointed out by Vincent et al. (2006). In comparison, the description of applications that can find their source of inspiration in geological processes is rather scarce in the literature. Most of these applications fall in the field of materials science and they are referred to as "geomimetics." In the dictionary of ceramic science and engineering (McColm, 2013), geomimetics is defined as "the science that uses preparative techniques to control composition and structure to copy minerals and improve their properties." According to this definition, the engineering interest behind geomimetics resides in the properties of the natural material itself rather than in the way this material is formed in nature.

Studies dealing with the reproduction of geological processes for technical purposes are rather defined as "geo-inspired" or as "mimicking nature" (e.g., Camblor, 2006; Okada et al., 2011; Aresta et al., 2014; Ruiz-Agudo et al., 2014). As shown by Fratzl and Barth (2009) for biomaterials, the use of nature as a source of inspiration for the design of functional materials builds bridges between materials science and biology. These bridges may in turn contribute to shed new light on the biological functions of the natural material itself. The present contribution follows the same approach by using a geochemical process as a source of inspiration for materials science and engineering with the additional aim of better understanding the natural process itself.

The starting point for considering the geo-inspired valorization of steel slags is the production of two valuable compounds, H_2 and magnetite, in the course of a geochemical process, called serpentinization, where iron-bearing refractory minerals are oxidized through their interaction with hot seawater. Steel slags are also composed of refractory minerals with ferrous iron being mainly hosted by magnesio-wüstite (Fe,Mg)O. By analogy, these anthropogenic materials have the potential to produce H_2 and magnetite as well. The geo-inspired strategy here is driven by the environmental benefit of using wastes for producing H_2 with limited (or even negative) CO_2 emission, and magnetite which exhibits surface properties that are suitable for the treatment of polluted water, effluents and soils. Obviously, the smaller the magnetite grain size, the higher the magnetite specific surface area and the more

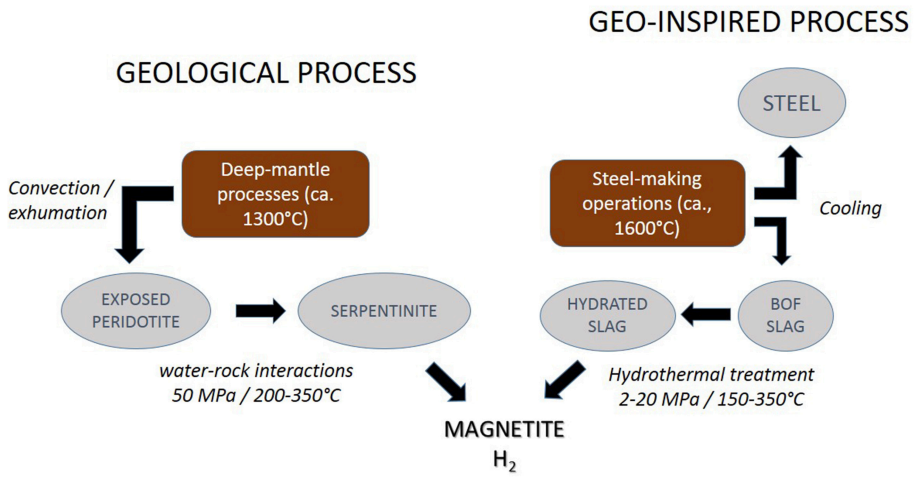

FIGURE 1 | General scheme of H_2 and magnetite production by serpentinization and by its geo-inspired counterpart process which is based on the hydrothermal treatment of steel slags (here BOF).

suitable the magnetite for these environmental applications. Strictly speaking, nanoparticles are defined as particles with sizes below 100 nm. For convenience, magnetite with a diameter below 500 nm will be termed nanomagnetite here since the hydrothermal treatment of ferrous slags tends to produce magnetite with sizes in that range, i.e., far below the threshold where magnetite is no longer obtained industrially through direct crushing of the ore (e.g., Corrans and Angove, 1991). Magnetite below 1 μm is usually obtained by chemical methods. The synthesis of nano-magnetite at the industrial scale is achieved by the Laux method, where nitrobenzene is reduced into aniline by cast iron to form magnetite. Other methods, mostly developed at the laboratory scale, involve the precipitation of stoichiometric Fe^{2+}/Fe^{3+} salts or the oxidation/reduction of iron salts/oxides under near-ambient conditions (e.g., Regazzoni et al., 1981). Nanomagnetite with monodisperse size distribution in the 10–20 nm range can be obtained from this type of method. Further hydrothermal treatment is required to achieve larger grain sizes (e.g., Daou et al., 2006). For example, (Mao et al., 2006) obtained monodisperse magnetite with sizes close to 500 nm with very regular morphology from hydrothermal treatment at 180°C of iron powder over 24 h. Industrial magnetite nanoparticles are mainly used as pigment and toner. Owing to remarkable magnetic and chemical properties, magnetite nanoparticles, either functionalized or not, can be potentially used in a wide range of applications: contaminant sorption and/or degradation, ferrofluids, magnetically guided drug delivery, electromagnetic wave absorbent, etc. (Blaney, 2007 and references therein). It may therefore be anticipated that the magnetite nanoparticles market will expand in the forthcoming years, in particular if manufacturing costs are reduced.

H_2 production is very much dominated by the transformation of fossil fuels (gas- and oil-reforming, coal gasification); <5 percent of overall H_2 production is achieved by other means (Ewan and Allen, 2005), i.e., water electrolysis and, to a much lesser extent, biomass. In other words, today, H_2 production is accompanied by substantial CO_2 emissions, i.e., 1 mole CO_2 for 4 moles of H_2 in the case of steam-methane reforming. A shift toward H_2 production from renewable (e.g., solar, wind) is therefore required for H_2 to become a true low-carbon energy and, consequently, a major player of the energy transition. In view of the expected growing importance of H_2 in the energy mix, alternative H_2 production methods are being considered, or even re-considered—as in the case of the steam-iron process which yields H_2 (and magnetite) as end-products. This industrial process, which was operated at the beginning of the 20th century, used the oxidation of iron in the presence of steam to produce H_2. At the time, pure H_2 was used as a "lighter-than-air" gas for lifting tethered balloons until it was replaced by helium in the early 30s (Williams, 1980). The steam iron method relies on a chemical-looping process, where an iron oxide is reduced by the carbon monoxide of gasified coal in a first step; then, this reduced form of iron (oxide or metal) is reacted with steam and iron re-oxidizes by splitting water to produce H_2 (e.g., Hacker et al., 2000; Lorente et al., 2011). The net reaction corresponds to the water-gas shift: $COg + H_2Og \Rightarrow CO_2 + H_2$ (e.g., Murugan et al., 2011), with oxygen being transiently stored in the form of iron oxide. There is therefore the potential to use embarked cartridges of reduced iron to produce H_2-rich steam for remote production and utilization (e.g., Azad et al., 2008). Whereas, in the early 1900s, H_2 was produced with the Lane producer, which operated at temperatures around 600–800°C, new versions of steam-iron producers can be operated in the same T range (stable cycle at 900°C) with gasified biomass using sponge iron with a high surface area to yield high-purity H_2, compatible with fuel-cell applications (Hacker et al., 2000). Another approach would consist in using a low-value ferrous starting material to achieve water splitting without considering further reduction steps. The steel industry does produce such potential starting materials (waste, byproducts, mine tailing), the H_2-production capacity of

which has already been investigated in a few experimental studies (Azad et al., 2008; Matsuura and Tsukihashi, 2012; Malvoisin et al., 2013; Michiels et al., 2015, 2018; Shatokha et al., 2016; Crouzet et al., 2017b; Kularatne et al., 2018 for olivine-bearing mine tailings of nickel extraction). The steam-iron process can be categorized as a thermochemical water-splitting method which uses iron as reducing agent. Finally, and it is the core of the present contribution, serpentinization reactions which occur in nature do also achieve thermochemical water splitting along with the production of magnetite. Our understanding of H_2 and magnetite production can thus potentially benefit from the scientific knowledge gained by the geochemical community on serpentinization reactions, knowledge that can ultimately be a source of inspiration for designing and optimizing engineered H_2, and magnetite production at a large scale.

OLIVINE SERPENTINIZATION: THERMOCHEMICAL FRAMEWORK

H_2/Magnetite-Forming Hydrothermal Reactions

In the sixties already, serpentinization reactions that result in the formation of serpentine group minerals from the interaction between water and ultramafic rocks were recognized as potential H_2-producing reactions. When writing serpentinite-forming reactions from olivine + water and enstatite + water, Thayer (1966) balanced the oxidation of Fe^{2+} contained in the reactant into Fe^{3+} in magnetite by considering the formation of H_2. In one review paper on the serpentinization of ultramafic rocks, Moody (1976) related the occurrence of native iron and iron-nickel alloys to highly reducing conditions implying H_2O-H_2 fluids. Native H_2 emanation and seepage associated with mafic/ultramafic rocks have been described for both oceanic (e.g., Welhan and Craig, 1979; Charlou and Donval, 1993; Kelley et al., 2001; Charlou et al., 2002) and continental settings (e.g., Neal and Stanger, 1983; Coveney et al., 1987; Abrajano et al., 1988, 1990; Sano et al., 1993; Zgonnik et al., 2015; Deville and Prinzhofer, 2016). The possibility of producing H_2 in the course of fluid/rock interactions is supported by experimental data (e.g., Janecky and Seyfried, 1986; Allen and Seyfried, 2003; Marcaillou et al., 2011) and thermochemical calculations (Wetzel and Shock, 2000).

For temperatures below ca. 350–400°C at 50–100 MPa, olivine is no longer stable in the presence of water and tends to form hydrous minerals (serpentine-group minerals and brucite) according to the following simplified reaction:

$$2Mg_2SiO_4 + 3H_2O \Rightarrow Mg_3Si_2O_5(OH)_4 + Mg(OH)_2 \qquad (1)$$

Similar reactions can be written from orthopyroxene reacting with water to form serpentine and talc. These simplified reactions do not account for the presence of Fe^{2+} in both olivine and pyroxene, which modifies the above phase relationship by introducing Fe_3O_4, magnetite.

Reaction 1 with Fe-bearing olivine writes following Evans (2008):

$$\begin{aligned}(Mg, Fe)-\text{olivine} + H_2O \;\Rightarrow\; &(Mg, Fe)-\text{serpentine} + (Mg, Fe)\\ &-\text{brucite} + \text{magnetite} + H_2 \qquad (2)\end{aligned}$$

The introduction of H_2 in the products of Reaction (2) or the introduction of O_2 in the reactants, results from the fact that part of the iron contained in both magnetite and serpentine occurs as Fe^{3+}, whereas only Fe^{2+} is initially present in olivine. Reaction (2) can also write in a very simplified manner as a sum of two half redox reactions between the FeO component in olivine, $[FeO]^{\circ olivine}$, and the Fe_2O_3 component in magnetite and/or serpentine, $[Fe_2O_3]^{mag,serp}$, in order to emphasize the oxidation of ferrous iron contained in olivine:

$$\begin{aligned}2[FeO]^{\circ olivine} + 1/2O_2 &= [Fe_2O_3]^{mag,serp}\\ H_2O &= H_2 + 1/2O_2\\ \text{---------------------------------}&\\ 2[FeO]^{\circ olivine} + H_2O &= [Fe_2O_3]^{mag,serp} + H_2 \qquad (3)\end{aligned}$$

Besides the issues of the natural synthesis of H_2-rich fluids venting at mid-oceanic ridges and their role as a fuel for deep-sea microbial communities (e.g., Kelley et al., 2005; Flores et al., 2011), serpentinization of the oceanic lithosphere dramatically modifies its physical and chemical properties. Hence, serpentinization reactions have been the subject of numerous thermodynamic and kinetic studies.

Effect of Temperature on Serpentinization

Olivine serpentinization and subsequent H_2 and magnetite production, is a thermally activated process. However, at a few tenths of MPa and for temperatures above 350–400°C, the reaction will cease because serpentine thermal stability limit is approached. Kinetically, the optimal reaction temperature results from the competition between decreasing thermodynamic driving force and increasing thermal activation. Accordingly, reaction kinetics follow a bell-shaped dependency on temperature. The corresponding optimal temperature has been determined experimentally on synthetic forsterite, Mg_2SiO_4, by Martin and Fyfe (1970) and Wegner and Ernst (1983) as well as on San Carlos (SC) olivine by Malvoisin et al. (2012a) and was found to be around 260, 300, and again 300°C, respectively. A synthetic plot of the olivine conversion rate as a function of temperature for the experimental datasets available in the literature is found in McCollom et al. (2016, Figure 13). On the low-temperature side, modeling by Klein et al. (2013) shows that serpentinization of olivine with composition close to Fo90 does not yield magnetite when temperature is below about 200°C; iron is then distributed among brucite and serpentine. For their calculation, Klein et al. (2013) used the SUPCRT92 database (Johnson et al., 1992), to which they added the thermodynamic data for greenalite and minnesotaite from McCollom and Bach (2009) and for ferroan brucite (Klein et al., 2009) in order to account for the ferrous iron end-member of chrysotile, talc, and brucite solid-solutions,

respectively. Solid solutions are considered by the authors as ideal, and serpentine compositions are calculated assuming four end-members—chrysotile, kaolinite, greenalite, and cronstedtite.

The customized database used by Klein et al. (2013) predicts that H_2 should, however, still be produced below 200°C due to the fact that most of the iron in serpentine is hosted as Fe^{3+} under these conditions. This notion is supported by data on serpentinized oceanic samples (e.g., Klein et al., 2014). Marcaillou et al. (2011) submitted natural peridotite samples to hydrothermal alteration at 300°C and 30 MPa for 70 days. They showed that, despite the highly reducing conditions evidenced by the formation of H_2, the serpentinite product displays a $Fe^{3+}/\Sigma Fe$ ratio that is similar to that of magnetite. Although the thermochemical calculation by Klein et al. (2013) nicely predicts H_2 production at temperatures below 200°C despite the absence of magnetite, it must be recalled that the thermodynamics of the pivotal phase of the corresponding model, namely serpentine, is highly simplified and that an ideal solid-solution model is considered between end-members with thermodynamic parameters that are mostly approximated (Klein et al., 2009, 2013; McCollom and Bach, 2009). McCollom et al. (2016) pointed out that existing thermodynamics models fail at accurately predicting iron distribution among the products of olivine serpentinization experiments, which basically controls H_2 and magnetite production yields. The issue of the consistency between thermodynamic models and experimental data with respect to olivine serpentinization remains to be further addressed. At even lower temperatures, below 150°C, the way H_2 can be produced remains difficult to apprehend from equilibrium thermodynamics due to major kinetics control even at geological timescales. Low-temperature H_2 production from natural and synthetic rock samples is therefore also difficult to achieve experimentally. Experimental data are, however, available at T below 150°C which suggest that H_2 can still be produced through the formation of Fe^{3+} oxi-hydroxides (Mayhew et al., 2013), with H_2 formation being possibly catalyzed by the surface of spinel-structure minerals occurring in ultramafic rocks.

Kinetics Framework of Olivine Serpentinization

Serpentinization of the oceanic lithosphere can proceed when ultramafic minerals are contacted with hot seawater under appropriate pressure and temperature (PT) conditions. Therefore, depending on the PT conditions at which this contact takes place, serpentinization reactions can proceed more or less far from equilibrium, the kinetics of which can potentially be controlled by the rate of dissolution of the reactants, the rate of crystallization of the products and/or the rate of iron oxidation from Fe^{2+} to Fe^{3+}. With water being a reactant, the rate of the overall serpentinization process can be limited by the rate at which water is supplied to the rock system. In numerous studies, the serpentinization rate of the oceanic lithosphere is considered to be chiefly controlled by hydro-mechanical factors (e.g., Rudge et al., 2010; Malvoisin and Brunet, 2014; Rouméjon and Cannat, 2014). As far as thermochemical parameters are concerned, Malvoisin et al. (2012a) showed that the serpentinization kinetics of San Carlos olivine is inversely proportional to the geometrical surface area of the starting olivine and, therefore, olivine dissolution rate has been proposed to be the rate limiting step. However, for initial olivine grain sizes below 5 μm, the nature of the produced serpentine mineral switches from lizardite to chrysotile, and the relationship between geometrical surface area and kinetics is broken, suggesting that another reaction step has become rate-determining. The appearance of chrysotile can be seen as a response to increasing supersaturation due to the faster olivine dissolution rate for the smallest grain size. Indeed, on the basis of flow-through experiments on crushed San Carlos olivine at 300°C/30 MPa, Normand et al. (2002) pointed out that chrysotile nucleation is favored over lizardite nucleation toward higher supersaturation levels. Berndt et al. (1996) and McCollom et al. (2016) obtained chrysotile from olivine submitted to 50 MPa/300°C and 35 MPa/200–320°C, respectively. Both studies showed a silica content of the hydrothermal solution exceeding that of chrysotile saturation (**Figure 2**), i.e., close to the metastable brucite–olivine equilibrium (McCollom et al., 2016). Therefore, the crystallization of metastable chrysotile instead of lizardite upon faster olivine dissolution can be the result of this supersaturation effect and could be seen as an expression of Ostwald's step rule. Serpentine precursors like protoserpentine (Lafay et al., 2016 and references therein) might actually control the silica content of the solution at a concentration close to the brucite–olivine metastable equilibrium (**Figure 2**).

The relationship between olivine geometrical surface area and magnetite/H_2 production kinetics may somehow be misleading on the exact role of geometrical surface area. It has been shown that olivine hydration does produce new reactive surface area by grain fracturing in both nature and experiments (e.g., Andreani et al., 2007; Iyer et al., 2008; Jamtveit et al., 2009; Okamoto et al., 2011; Kelemen and Hirth, 2012; Lafay et al., 2012; Plümper et al., 2012; Rouméjon and Cannat, 2014; Shimizu and Okamoto, 2016; Malvoisin et al., 2017). Therefore, a larger surface than the mere outer shell of the grain is accessible to water and thus contributes to the overall reaction.

Most experiments performed on olivine serpentinization used either pure water or seawater, leading to pH conditions that are neutral or slightly basic (Malvoisin et al., 2012a; McCollom et al., 2016; Huang et al., 2017). The olivine dissolution rate at temperatures up to 150°C has been shown to decrease with pH in the 2–8 range (Wogelius and Walther, 1991; Pokrovsky and Schott, 2000; Hänchen et al., 2006). It is therefore expected that acidic pH must increase olivine serpentinization kinetics. On the other hand, Lafay et al. (2012) showed that alkaline pH significantly increases the serpentinization rate of San Carlos olivine into chrysotile, whereas it has been shown that beyond 8, the olivine dissolution rate is minimal (Pokrovsky and Schott, 2000; Hänchen et al., 2006) with no more pH dependency. The rate-determining steps of the olivine serpentinization and their T and pH dependency still remain to be determined.

Another parameter that has been proposed as major control over olivine serpentinization kinetics is the presence of minor metal cations such as Al^{3+} and Cr^{3+} (Andreani et al., 2013; Pens et al., 2016; Huang et al., 2017), which are basically present

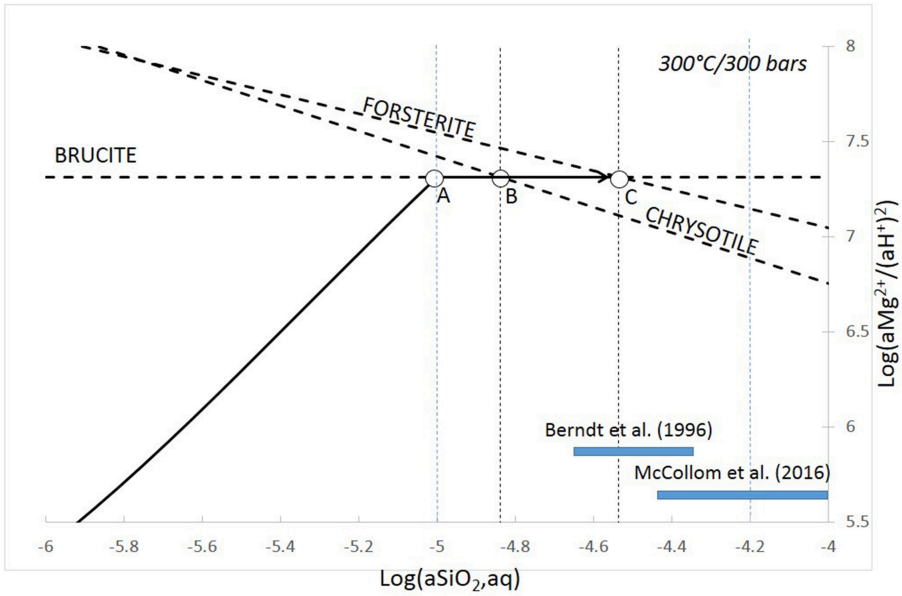

FIGURE 2 | Activity-activity diagram in the MgO-SiO_2-H_2O system showing the solubility limits of olivine–brucite and chrysotile. The plain line indicates a possible compositional path of the solution in response to olivine dissolution. In the constant equilibrium case, brucite would form at Point A and the solution composition should evolve until Point B, where the stable assemblage brucite + chrysotile would precipitate. Assuming that chrysotile does not form, then the composition may reach the metastable Point C, where olivine saturation is achieved. The silica concentration range (assumed here to equate to silica activity) measured in the aqueous solution of hydrothermal experiments performed at 300°C with Fe-bearing natural olivine as starting material (Berndt et al., 1996 and McCollom et al., 2016), are reported. They are consistent with buffering by the olivine–brucite metastable equilibrium (McCollom et al., 2016).

in natural systems but sometimes absent from experimental ones. The presence of aqueous Al is believed to promote olivine dissolution (Pens et al., 2016).

The Role of the Water-To-Rock Ratio

Finally, both experimental work and thermochemical modeling emphasize the prominent role of the water-to-rock mass ratio in the serpentinization process. This parameter is of relevance for the natural process since serpentinization of the oceanic lithosphere is a chemically open system (e.g., Decitre et al., 2002; Boschi et al., 2008; Vils et al., 2009; Malvoisin, 2015) that is powered by the convection of seawater. The water-to-rock ratio required to transform a peridotite into a serpentinite largely exceeds the water-to-rock ratio corresponding to a close system of saturated porosity. Indeed, the water-to-rock ratio can be seen as a parameter that characterizes the magnitude of the water–rock interaction or the chemical openness of the natural system. In batch experiments such as those that will be presented below, the solution is not renewed so, strictly speaking, the experimental system is chemically close. However, typical water-to-rock mass ratios of 10–100 are usually investigated, and the total mass of dissolved species in the aqueous solution may become significant and may require consideration in mass balance calculations. Although significant mass transfer from mineral phases to aqueous solution can then be achieved, the aqueous species remain available for further reaction, in contrast to a true open system. Olivine hydration in a true open system has been the subject of reactive percolation experiments through a sintered porous aggregate (Godard et al., 2013) for water-to-rock ratios typically reaching up to 20. This approach allows for the investigation of coupling between mineral reaction-kinetics and hydrodynamics, two main parameters that are likely to control serpentinization rates in natural settings.

HYDROGEN AND MAGNETITE PRODUCTION FROM HYDROTHERMALLY PROCESSED STEEL SLAGS: PREVIOUS STUDIES

Steel Slag Composition and Mineralogy

Two main types of slags are produced by the steelmaking industry during the refinement processes which consist of transforming and purifying the iron ore to produce steel. These processes involve high temperatures—typically above 1,300°C—and redox reactions, since the iron ore mostly contains ferric iron whereas the steel is composed of iron metal. The high temperature operations are powered by the combustion of coke and coal with pre-heated air. This combustion reaction produces carbon monoxide, which subsequently reduces iron with carbon dioxide as a byproduct. A large amount of calcium carbonate is added to the blast furnace in order to act as a flux and to concentrate impurities in the liquid to form a liquid slag. Sulfur, which is incorporated with the coke, tends to dissolve in the liquid metal. However, due to its strong affinity for Ca, sulfur concentrates in the liquid slag. Blast furnace slags (BF)

are rich in CaO, SiO_2, Al_2O_3, and MgO components, which are incorporated upon cooling into calcium silicates such as merwinite or melilite group minerals. The FeO content of the BF slags is below 1 wt%, and this type of slag is therefore not suitable for the valorization strategy presented here. BF slags are largely valorized for their hydraulic cementitious properties. The molten metal contains several wt% of carbon and requires further refinement to reach the expected steel quality. A steelmaking process is therefore further carried out in a basic oxygen furnace (BOF) following the Linz and Donawitz process. Again, high temperature operations in the 1,600–1,650°C range are carried out and a pure oxygen stream is blown on the charge in order to remove the impurities through intense oxidation reactions. Carbon, for example, is removed as carbon monoxide. As for the blast furnace operation, CaO-rich fluxes or slag formers are added to concentrate the impurities in the liquid BOF slag, which floats above the molten metal. In comparison to BF, BOF slags have a higher iron content under both Fe^{2+} and Fe^{3+} oxidation states, which results from the oxidation conditions in the BOF. The total iron content in BOF slags is typically comprised between 10 and 30 wt% FeO (see the compilation by Yildirim and Prezzi, 2011). Ferrous iron is mainly incorporated in the magnesio-wüstite solid-solution (Mg, Fe)O. Ferric iron is hosted by magnetite and calcium-ferrite structure-type minerals, with intermediate compositions between srebrodolskite, $Ca_2Fe_2O_5$, and brownmillerite, Ca_2AlFeO_5 (e.g., Malvoisin et al., 2013). This latter mineral group is of environmental importance since it concentrates chromium and vanadium (Chaurand et al., 2006).

Steel slags are also produced from the Electrical Arc Furnace (EAF) steelmaking process. EAF is fed with steel scraps and pig iron, which are molten along with carbonate fluxes using a high-power electric arc. In the refinement stages, oxygen is injected to oxidize and remove part of the impurities dissolved in the liquid metal. The resulting EAF slag has an overall composition which resembles that of BOF slags, with CaO, FeO, Al_2O_3, and SiO_2 as main constituents (Ter Teo et al., 2016). However, the composition of EAF slags can be subjected to substantial variations since it depends on the chemistry of the steel scraps that are fed into the electrical-arc furnace. Mineralogical characterization of various EAF slags shows that, as in BOF slags, iron is both divalent and trivalent and hosted in spinel-structure phases (including magnetite), Mg-bearing wüstite, and substituted brownmillerite (Mombelli et al., 2016 and references therein).

Overall, steel slags have the complexity of a natural rock. Compared to ultramafic rocks, the composition of steel slags is dominated by CaO, which is mainly hosted by $Ca(OH)_2$ and $CaCO_3$ phases. These secondary minerals form from lime reaction with atmospheric water and carbon dioxide. Crouzet et al. (2017b) analyzed three slag samples with various storage times in air on their production site. They showed that mass loss on ignition, CO_2 content and Fe^{3+}/Fe_{total} ratio increase with storage time, the later value being comprised between 55 and 66%. The presence of portlandite, $Ca(OH)_2$, implies that when the slag is contacted with pure water, even when ambient, pH readily increases to ca. 11.

Monitoring Steel Slag Oxidation Under Hydrothermal Conditions

As already mentioned, steel slags and, more generally, steel industry byproducts have a variable iron content depending on the way they are produced. In order to be able to compare the H_2 (or magnetite) production rate among these different materials, it is convenient to define its intrinsic H_2 production capacity (HPC). The HPC is expressed here in g H_2/kg and corresponds to the total mass (g) of H_2 that can be potentially produced by kg of the FeO-bearing sample. Based on the following iron oxidation reaction:

$$3FeO + H_2O \Rightarrow Fe_3O_4 + H_2 \qquad (4)$$

The HPC of pure FeO is calculated to amount to 9.3 g H_2/kg, which is basically the highest HPC that can be achieved from any FeO-bearing starting material containing no iron metal.

Assuming that H_2 is only produced according to Reaction (4), the HPC of a given steel slag (HPC_{slag}) containing a mass fraction of FeO (X_{FeO}) can then be calculated as $HPC_{slag} = 9.3 \cdot X_{FeO}$. The FeO content of abyssal peridotites is lower than 10 wt% (e.g., Baker and Beckett, 1999; Niu, 2004), corresponding to an HPC below 1 g H_2/kg. For comparison, an average BOF steel slag contains around 20 wt.% FeO (see previous section), corresponding to an HPC of ca. 2 g H_2/kg.

In order to investigate the H_2 production potential of BOF steel slags, Malvoisin et al. (2013) reproduced the experimental approach developed for the study of San Carlos olivine hydration (Malvoisin et al., 2012a,b). Steel slag powder was enclosed with deionized water in gold tubes welded shut. Temperatures comprised between 473 and 673 K, were investigated at 50 MPa by introducing the gold capsule containing the sample in an externally heated cold-seal vessel (Brunet and Chopin, 1995). After the experiment at the nominal P-T conditions, the vessel is cooled down with a compressed air stream and near ambient temperature is attained within about 30 min. The recovered gold capsule which sustains a slight overpressure is pierced inside a syringe (Malvoisin et al., 2013). The experimental gas mixes into the argon volume that fills the decompression syringe. The obtained H_2-bearing argon gas is injected into the column of a gas chromatographer. Malvoisin et al. (2013) also applied to their treated BOF slag samples the magnetic method which was successfully applied to the quantification of magnetite production in the course of San Carlos olivine hydrothermal alteration (Malvoisin et al., 2012b). The authors determined the amount of magnetite from the saturation magnetization (Js) of the hydrothermally treated slag. The near one-to-one correlation obtained by Malvoisin et al. (2013) between the number of moles of both magnetite and H_2 produced over a range of reaction progresses of up to 50% confirmed Reaction (4).

In addition to experiments in sealed gold capsules, Crouzet et al. (2017b) used a stirred sampling autoclave equipped for both gas and solution sampling. Dissolved iron as well as H_2 concentration in the gas phase could be monitored *in situ* in the course of hydrothermal treatment of the BOF slag. Both water and FeO samples were loaded in the autoclave beforehand, and argon was injected into the headspace to pressurize the system

at conditions above P*sat* so that water mostly remained liquid. Although sampling autoclave offers a convenient way to monitor the *in-situ* production of H_2, the metal of the autoclave cannot sustain the same extreme pH conditions as gold capsules. Taking into account that acidic conditions favor FeO dissolution kinetics (Jang and Brantley, 2009) which, in turn, speeds up the H_2 production (Crouzet et al., 2017a), the resistance of the metal of the reaction vessel may become limiting regarding a strategy that would use very low pH to improve the hydrothermal reaction kinetics. On the other hand, the kinetics improvement gained by using acidic conditions allows for the achievement of an acceptable run duration (Crouzet et al., 2017a,b) at temperatures that are sustained by PTFE liners inserted in the sampling autoclave. Finally, it must be noted that Crouzet et al. (2017a) used both gold capsules and a sampling autoclave. They obtained a relatively higher H_2 yield when using the sampling autoclave. This discrepancy was interpreted as resulting from the effect of stirring on reaction rates, which promotes chemical exchange between solid and solution.

Mineralogical Evolution After Hydrothermal Treatment

The studies by Malvoisin et al. (2013) and Crouzet et al. (2017b) showed how the initial mineralogy of a BOF steel slag is modified by the hydrothermal treatment (**Figure 3**). The major effect of the hydrothermal treatment is the hydration of the slag with the formation of calcium silicate hydrates and calcium aluminous silicate hydrates along with portlandite in the case of a fresh slag initially containing residual lime (Malvoisin et al., 2013; Crouzet et al., 2017b). Another important effect with respect to H_2 formation is the overall oxidation of the slag as evidenced by an increase of the $Fe^{3+}/(Fe^{2+}+Fe^{3+})$ ratio. The iron containing phases in the starting slag are wüstite (Fe,Mg)O, iron metal and brownmillerite, a Fe^{3+}-bearing mineral. In the hydrothermally treated slag (**Figure 3**), the abundance of magnetite and hibschite strongly increases. Malvoisin et al. (2013) showed that the evolution of the molar fraction of $Fe^{3+}/\Sigma Fe$ is mainly due to the oxidation of wüstite into magnetite, whereas the Fe^{3+} contained in brownmillerite is transferred to the newly formed hibschite. The oxidation of the BOF slag led to the production of up to 0.9 g H_2/kg slag. Since the HPC of the studied slag amounted to around 1.9 g H_2/kg, the maximum reaction extent achieved by Malvoisin et al. (2013) approached 50% at 50 MPa, 573 K, and 216 h. At the same temperature, Crouzet et al. (2017b) studied the oxidation of a BOF steel slag of different origin. They obtained a reaction extent of 20% after 3 days. An increase of the temperature by 50°C led to a reaction extent of 75% after the same reaction time. The effect of grinding the slag down to particle sizes below 50 μm was found to be marginal, with a kinetics enhancement of only a factor of ca. 1.5 (Malvoisin et al., 2013; Brunet et al., 2014). Although Malvoisin et al. (2013) used magnetite amount as a proxy of H_2 production as quantified using magnetic methods, they did not pay much attention to the size distribution of the magnetite grains. SEM imaging of magnetite was mostly aimed at tracking Reaction (4) at the micro-scale through the study of the textural relationship between reacting wüstite and growing magnetite.

MODELING STEEL SLAG HYDROTHERMAL OXIDATION BASED ON WÜSTITE THERMOCHEMISTRY

Since ferrous iron is mostly present as wüstite in BOF slags, the oxidation behavior of pure FeO under hydrothermal conditions will be used as a reference to predict that of FeO contained in steel slags. In other words, it will be considered that although the other chemical components of the slag may change the physicochemical conditions (e.g., pH and ionic strength), the processes operating in the pure FeO–water system will remain applicable. The purpose here is to use thermodynamic calculation on pure FeO as a guideline for the optimization of the physico-chemical conditions in the perspective of an industrial process. The main objection to the strategy of using pure FeO as an analog of ferrous iron in slag is the presence of significant magnesium in the wüstite component of BOF slags which may, however, be accounted for by an activity term for FeO in wüstite. The possible kinetics effect of the presence of magnesium remains to be investigated as that of the impurities contained in wüstite.

A parameter of paramount importance for the industrial production of magnetite and H_2 is the timescale of the process. A rate-law for FeO dissolution was retrieved and implemented in PHREEQC for thermochemical modeling. The pH dependency of this rate law was taken from Jang and Brantley (2009). Evolution of the FeO surface area was calculated assuming a constant grain population through time with identical radii. A term (1-Q/K) was added to account for the effect of FeO saturation index on its dissolution kinetics (e.g., Lasaga, 1984). It was assumed that the rate of H_2 production from wüstite oxidation in Crouzet et al. (2017a) was controlled by wüstite dissolution kinetics at 150°C, 15 MPa with 0.05 M acetic acid; an E_a of 50–60 kJ.mol^{-1} is obtained using the constraint that H_2 production is achieved within about 7 h under the aforementioned conditions (Crouzet et al., 2017a). With this rate law which reproduces the iron flux upon FeO dissolution at 25°C at pH < 6 (Jang and Brantley, 2009), and which reproduces the run duration required to reach completion in the 150°C experiment described in Crouzet et al. (2017a), the effect of pH, temperature and solid/water mass ratio on reaction kinetics and H_2/magnetite yield can be modeled (**Figure 4**). It must be recalled here that the (1-Q/K) term accounts for situations where FeO saturation is being approached. In most cases, however, the solution composition is maintained far from FeO saturation due to the precipitation of magnetite, which is the most stable iron oxide in the system for a wide range of f_{H2} (see Discussion).

Effect of pH, Temperature, Starting Material/Solution Mass Ratio, and Pressure on FeO Oxidation

The effect of decreasing pH is two-fold. First, it increases the kinetics of FeO dissolution, and H_2 and magnetite production rates are consequently enhanced. Second, decreasing

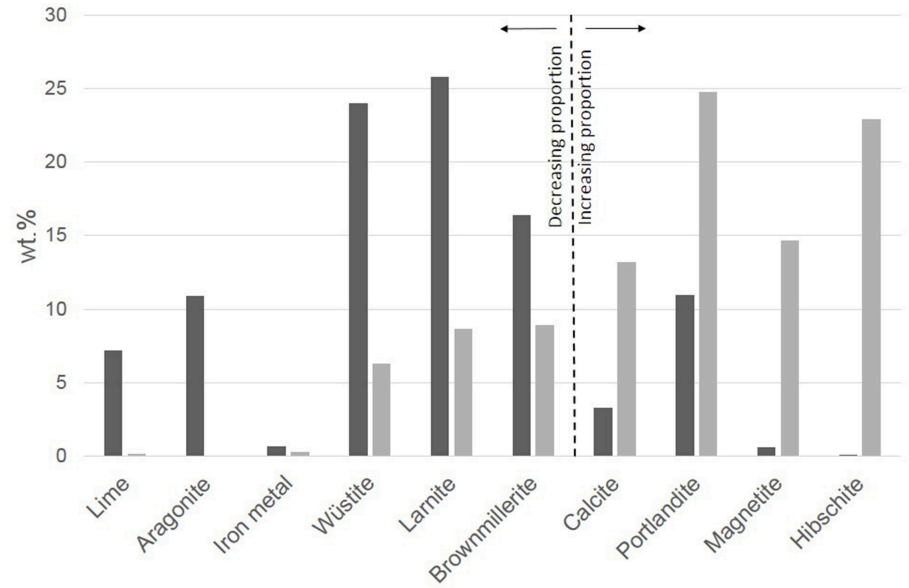

FIGURE 3 | Evolution of the mineralogy of a BOF slag treated hydrothermally at 50 MPa and 573 K for 216 h. *Black sticks*: mineralogical composition of the starting material; *Gray sticks*: Hydrothermal run product. Data are from Malvoisin et al. (2013).

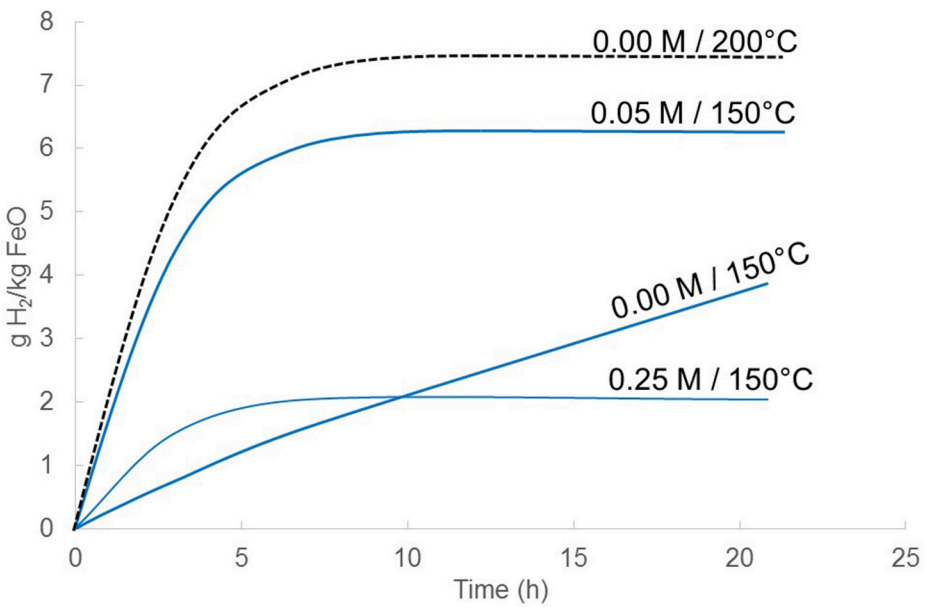

FIGURE 4 | Effect of temperature and acid acetic concentration on H_2 production kinetics and yield. The H_2 yield (g/kg FeO) is modeled for a solid-to-solution mass ratio of 1:200. For the calculation, initial water volume is fixed to 200 mL, corresponding to a headspace of 300 mL. Temperature is 150°C and 200°C, pressure is 15 MPa. Higher solid-to-solution mass ratio implies a lesser proportion of the initial FeO that is dissolved; accordingly, the H_2 yield is higher. The H_2 yield is modeled for acid acetic concentrations of 0, 0.05, and 0.25 M. Note that the highest concentration (0.25 M) produces less H_2 since a larger proportion of Fe resides in the solution and does not produce magnetite.

pH increases iron solubility. For a given amount of solution, more Fe^{2+} is dissolved into the solution that will no longer react to produce H_2 and magnetite. On **Figure 4**, H_2 yield from FeO oxidation at 150°C for a solution-to-solid mass ratio of 200 is plotted as a function of time for three acetic acid concentrations (0, 0.05, and 0.25 M) corresponding to equilibrium pH of ca. 6.3, 4.7, and 4.5, respectively. It can be seen that the H_2 production rate is strongly increased when acetic acid is added, while H_2

yield drops. Maximum H_2 yield can, however, be compensated by decreasing the solution-to-solid mass ratio (**Figure 4**).

Temperature has two main effects on hydrothermal wüstite oxidation. First, it increases reaction kinetics, and second, it decreases iron solubility. In other words, increasing temperature will enhance magnetite (and H_2) yield at a given run duration by speeding up the reaction and by lowering the amount of unreacted (divalent) iron present in the solution. The addition of acetic acid also increases the overall reaction kinetics (**Figure 4**)—at least as long as wüstite dissolution is the rate-determining step—by lowering the pH. However, consecutively to the pH decrease, more aqueous iron is present in the solution and less magnetite (and H_2) is hence produced.

The effect of temperature on H_2 production from pure FeO and BOF slags can be compared by plotting literature data on an Arrhenius plot (**Figure 5**). A first remarkable result is that the two studied BOF slags (Malvoisin et al., 2013 and Crouzet et al., 2017b) yielded significantly different E_a, differing by a factor of three. Crouzet et al. (2017b) found good consistency between the two studies, probably because they erroneously divided the true E_a obtained from their experiments by a factor of two. A second remarkable result is that in the 250–300°C range, reaction rates are almost identical for the two slags, furthermore they compare very well with the data obtained on pure FeO within the same temperature range. This consistency is striking since pH conditions, FeO grain-size and composition are expected to differ significantly among these experiments. Either this consistency is purely fortuitous or the rate-determining step in the 250–300°C range is little sensitive to the parameters listed above. Finally, there is apparently good consistency between the E_a obtained for BOF slag studied by Malvoisin et al. (2013) and FeO (Crouzet et al., 2017a), which may indicate that the rate-determining process is the same in the two cases. Unexpectedly, the E_a derived here for FeO hydrothermal oxidation at pH below 6 is twice that derived by Crouzet et al. (2017a) at pH close to 6. In both cases, the E_a is little constrained and the kinetics parameters of FeO hydrothermal oxidation might be pH-dependent—such is the case, for example, for albite dissolution (Hellmann, 1994).

The effect of pressure has not yet been systematically investigated experimentally. Experiments already published on the hydrothermal oxidation of FeO were performed between 20 and 50 MPa in the liquid water field. However, an important question which has not been addressed yet is whether the corresponding kinetics data extrapolate down to the pressure of the liquid water–vapor equilibrium (Psat). Indeed, working at Psat is convenient since pressure can be generated by water expansion upon heating without additional compression. Since the hydrothermal oxidation of FeO involves the production of a compressible phase, H_2, its equilibrium constant must be sensitive to pressure. However, since the hydrothermal reaction occurs far from equilibrium, it has been implicitly considered (Brunet et al., 2014) that decreasing pressure down to Psat should not affect significantly the driving force of the reaction and, hence, its kinetics. Furthermore, dissolution–precipitation processes that are expected to be rate determining, should not be affected by changes in the gas phase density and viscosity due to variations of pressure and of vapor content (higher at Psat) since solid reactants remain immerged in liquid water even when run at Psat.

The Determining Step of the Reaction Rate and Optimal Conditions

Crouzet et al. (2017a) analyzed both aqueous iron and produced H_2 in an experiment where reagent grade FeO (50–100 μm) was reacted with 0.05 M acetic acid solution at 150°C and 15 MPa. They basically achieved magnetite supersaturation due to the FeO dissolution rate, which exceeded the magnetite production rate. The authors therefore concluded that the reaction rate was controlled by Fe^{2+}, aq oxidation and/or magnetite precipitation. Considering that reaction completion was achieved in ca. 7 h (Crouzet et al., 2017a), an average magnetite production rate of around 1 $g.L^{-1}.h^{-1}$ can be calculated considering a solid-to-solution mass ratio of 1:200. The fact that the time required for the consumption of all the starting FeO nearly matches the end of the H_2 production stage (magnetite precipitation) suggests that near-optimal kinetics conditions have been achieved. In other words, although higher acetic acid concentrations may have further increased the FeO dissolution kinetics, overall magnetite (and H_2) production kinetics may not have increased accordingly since FeO dissolution is no longer the rate-determining step. The threshold of 1 $g_{Fe3O4}.L^{-1}.h^{-1}$ at 150°C gives an interesting estimate of optimized magnetite production rates at this temperature. If these production rates would not depend on the solid-to-solution mass ratio, an industrial installation containing 40 m^3 of 0.05 M acid acetic solution will be needed to produce around 1 ton of magnetite per day at 150°C from pure FeO.

Role of Impurities on the Reaction Kinetics and Implications for the Rate-Limiting Steps

There is so far no comprehensive experimental dataset on the effect of impurities on the formation of magnetite and H_2 from FeO-bearing slags. Michiels et al. (2015, 2018) studied the hydrothermal oxidation of Fe° contained in industrial wastes with the aim of producing H_2. Although iron is not divalent in their Fe-rich starting-materials, the oxidation route also involves iron oxidation, water splitting and magnetite precipitation. Michiels et al. (2015) showed that the addition of carbon dioxide under basic pH, which dissolves as CO_3^{2-}, promotes the oxidation of iron metal into magnetite at 160°C. Furthermore, Michiels et al. (2018) studied the effect on H_2 yield of a wide range of metal and oxide impurities as typically encountered in products of the steel industry. The authors identified reaction inhibitors that basically slow down the H_2 production. It is proposed that the inhibitors either promote the formation of a passivation layer around Fe° or they oxidize part of the Fe° starting material, which is then no longer available for water-splitting reaction. Probably more relevant to our concern, Michiels et al. (2018) identified Ni as a catalyst of the H_2 production reaction. Based on previous studies, Michiels et al. (2018) proposed that Ni catalyzes the water-splitting reaction, which is thus implicitly considered as the rate-limiting step. Magnetite production flux at 160°C increases from 4 to above 40 $g_{Fe3O4}.L^{-1}.h^{-1}$ when Ni is added

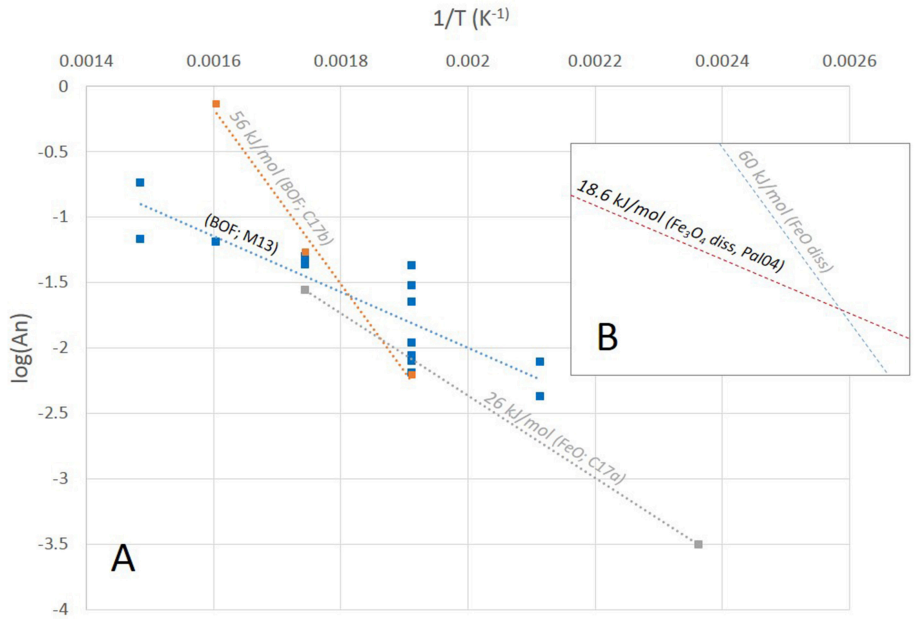

FIGURE 5 | Arrhenius plot of H_2 production reaction from BOF slag and pure FeO. **(A)** To be plotted, the H_2 production dataset by Malvoisin et al. (2013), or *M13*, has been fitted to the An.$t^{1/2}$ rate-law used by Crouzet et al. (2017a,b), indicated as *C17a* and *C17b*, respectively. Activation energies (Ea) have been retrieved; however, only the *M*13 dataset contains sufficient data to retrieve a reliable activation energy with its standard deviation (black font). *C17a* and *C17b* datasets is only based on 2 and 3 datapoints, respectively, and the derived Ea is thus only indicative (gray font). **(B)** For comparison, the dissolution kinetics of magnetite dissolution (and precipitation, Palandri and Kharaka, 2004; *Pal04*) is depicted by an idealized draw line, the slope of which is consistent with the E_a tabulated in *Pal04* using the scale of **(A)** plot. The E_a of FeO dissolution kinetics of ca. 60 kJ/mol is approximated by combining the room temperature dissolution data at pH < 6, published by Jang and Brantley (2009) and those at 150°C found in Crouzet et al. (2017a), see text body.

in optimized proportions (Michiels et al., 2018). Liu et al. (2016) studied the effect of HCl and Pd on the kinetics of hydrothermal H_2 (and magnetite) production from Fe° powder at 120°C. They showed the positive effect of adding acid due to an enhanced Fe° dissolution rate. At the level where acid addition was no longer beneficial (>0.02 M), H_2 (and magnetite) production kinetics could still be increased from 15 to 90 $g_{Fe3O4}.L^{-1}.h^{-1}$ by the deposition of a Pd catalyst onto Fe° grains. The data from Michiels et al. (2015, 2018) and Liu et al. (2016) in the 120–160°C range seem to indicate that above the threshold of a few grams per liter/day, the oxidation of iron metal into magnetite can still be enhanced by catalyzing water splitting (or the aqueous-iron redox-processes) using Ni or Pd. It might be worth investigating this catalytic option for FeO-rich starting materials as well.

DISCUSSION AND CONCLUSIONS

Grain Size Evolution of Magnetite in Hydrothermal Processes: Implications

The experimental studies by Crouzet et al. (2017a,b), on FeO and BOF slag hydrothermal oxidation, respectively, both yielded a magnetite fraction with sizes below 50 nm despite very different experimental conditions. In the first case, FeO experiments were run at 150°C, the acid acetic solution had an initial pH of 3 and aqueous Fe concentration indicated magnetite supersaturation (Crouzet et al., 2017a). In the second case (BOF slag), run temperature was 300°C with an initial pH of ca. 11 (Crouzet et al., 2017b).

Monodisperse nanomagnetite is mainly obtained using the co-precipitation method which is based on the simplified precipitation reaction:

$$Fe^{2+}, aq + 2Fe^{3+}, aq + 8OH- = Fe_3O_4 + 4H_2O \qquad (5)$$

Aqueous divalent and trivalent iron is supplied in stoichiometric amounts by soluble iron salts (e.g., $FeCl_2$ and $FeCl_3$). Addition of a base (e.g., ammonia) to the acidic solution composed of dissolved chlorides shifts the pH to higher values and drags Reaction (5) toward the precipitation of magnetite at near-ambient conditions. Nanomagnetite grains close to 10–20 nm are typically obtained with a size distribution that can be close to monodisperse when appropriate experimental conditions are applied. An additional hydrothermal step can be applied to increase the nanomagnetite grain size without altering monodispersity. As an example, Daou et al. (2006) increased the size of magnetite nanoparticles obtained from the co-precipitation method at 70°C, from 12 to 39 nm, by a further heating step in the same medium at 250°C for 24 h. Vayssières et al. (1998) showed that a way to tailor magnetite size is to control the ripening process after nucleation, which is enhanced by increasing temperature (25–45°C) but which is slowed down by increasing the ionic strength and/or the

pH of the aqueous crystallization medium at these temperature conditions. The opposite effect of temperature and pH may potentially explain why magnetite in the same size range is obtained under the contrasted conditions recalled above for the experiments of Crouzet et al. (2017a,b). Long et al. (2016) investigated the coarsening kinetics of magnetite nanoparticles produced by the co-precipitation method in the 100–200°C range. They found a linear dependency of magnetite diameter with time and determined an activation energy of around 30 kJ/mole. Magnetite nucleation and growth in aqueous solution has been investigated at the nm scale using cryo-TEM images by Baumgartner et al. (2013). They showed that the growth of precipitated magnetite proceeds by coalescence of elementary nanoparticles with initial sizes close to 2 nm. Furthermore, the particle diameter is found to increase linearly with time at 25°C, with a growth rate that decreases when pH is increased to the 9–11 range (Baumgartner et al., 2013). Magnetite growth-rate studies such has those outlined above should be extended to a larger range of temperature, pH and ionic strengths in order to be able to predict and thus tailor the size of magnetite grains obtained by the hydrothermal treatment of various iron-rich products.

Based on the experience gained on BOF slags and FeO, it would be expected that the growth of magnetite by coalescence and coarsening does also apply to serpentinization reactions. The evolution of magnetite grain-size (and content) as a function of serpentinization degree has been addressed by numerous studies dealing with the magnetic properties of serpentinized peridotites. Indeed, the magnetic grain size can be deduced from coercitivity and hysteresis parameters (e.g., Day et al., 1979; Dunlop, 1981). The correspondence between magnetite grain-size range and magnetite real grain-size must however be checked through petrographic observations (e.g., Oufi et al., 2002). It must however be noted that magnetic grain sizes encountered in serpentinized peridotites are often smaller than the size detection limit of conventional SEM devices used for petrographic investigations. Based on both petrographic and magnetic data, Maffione et al. (2014) proposed a model of magnetite grain-size evolution as a function of serpentinization degrees. They suggested that at the very first stages of serpentinization, magnetite grains are super-paramagnetic (SP) and single domain (SD), i.e., mostly composed of nanoparticles, whereas at higher serpentinization stages, magnetite grain sizes are larger. Magnetic investigation of serpentinized oceanic crust (Yokoniwa Rise, Central Indian Ridge) also revealed that slightly to moderately serpentinized samples show the presence of super-paramagnetic magnetite particles (Fujii et al., 2016), thus again consistent with the presence of magnetite nanoparticles. Malvoisin and Brunet (2014) exposed a San Carlos olivine aggregate to hydrothermal alteration and observed small magnetite grains ($\sim$1 μm) as well as larger magnetite aggregates. But again, the resolution of the SEM device used for the characterization had too low a resolution to identify nanoparticles of magnetite.

If the first percent of magnetite formed during serpentinization is composed of nanoparticules, their specific surface area can be 1,000 times higher than micrometer-size magnetite encountered at higher serpentinization degree. Accordingly, these magnetite grains formed at the early stages have the greatest catalytic potential at a stage where the fluid-to-rock ratio is still low (Maffione et al., 2014) and where H_2 content in solution is potentially the highest (Klein et al., 2009). In other works, abiogenic formation of reduced organic molecules catalyzed by magnetite surfaces (Berndt et al., 1996) could be the most efficient at these early serpentinization stages.

Hydrothermal Ferrous Iron Oxidation: Knowledge Gained From FeO, BOF, and Olivine Experiments

Sub-reaction (4) is relevant to both olivine serpentinization and steel slag hydrothermal oxidation considering the activity of the FeO component in olivine and magnesio-wüstite solid-solution in slags. Despite the presence of FeO in similar amounts (similar HPC), BOF slags and upper-mantle olivine significantly differ in their chemical composition. BOF slags are dominated by calcium oxide which imposes basic pH conditions when contacted with water. Dissolution of upper-mantle olivine, which is mostly composed of MgO and SiO_2, rather leads to circumneutral pH (McCollom et al., 2016). Olivine hydrothermal alteration products are mostly composed of serpentine along with magnetite. Since serpentine group minerals incorporate ferrous and ferric iron (e.g., Page, 1968), part of the FeO from olivine is not converted into magnetite, to such an extent that below 200°C, no magnetite is actually formed and all the ferric iron is contained in serpentine (Klein et al., 2009). In both hydrated slag, silica is bounded to Ca in the form of calcium silicate hydrates and Mg is incorporated into brucite, $Mg(OH)_2$ (Crouzet et al., 2017b), and no magnesium silicate is produced which could host iron in solid-solution. Crouzet et al. (2017c) showed, however, that under high CO_2 partial pressure, iron carbonate can form and sequester iron which is no longer available for magnetite formation.

A major characteristic of the phase relationships in FeO-Fe_2O_3-H_2O is the stability of magnetite under highly reducing conditions corresponding to H_2 saturation in water. In other words, when FeO is submitted to hydrothermal conditions, magnetite can keep forming along with H_2, even when the gas phase is composed of pure H_2. This behavior has been modeled by Crouzet et al. (2017a) at 150°C, and calculations using SUPCRT92 (Johnson et al., 1992) tend to show that this behavior should hold up to at least 250°C at 50 MPa. Therefore, below this temperature, the reaction will always remain non-reversible, since no equilibrium will be reached. Olivine serpentinization reaction is also non-reversible at 50 MPa up to around 350–370°C. The latter is also strongly exothermic (**Figure 6**), whereas pure FeO hydrothermal oxidation into magnetite is only exothermic below 250°C. Crouzet et al. (2017a) obtained optimal kinetics at 150°C in the presence of acetic acid. At this temperature, the reaction produces around 40 kJ/kgFe_3O_4 of heat; based on a Fe_3O_4 production rate of 10 g.L^{-1}.h^{-1}, a reactor of 1 m^3 (90 ton_{Fe3O4}/y) will only produce around 400 kJ/h or 110 watt. In the case of fresh steel slags, however, a strong

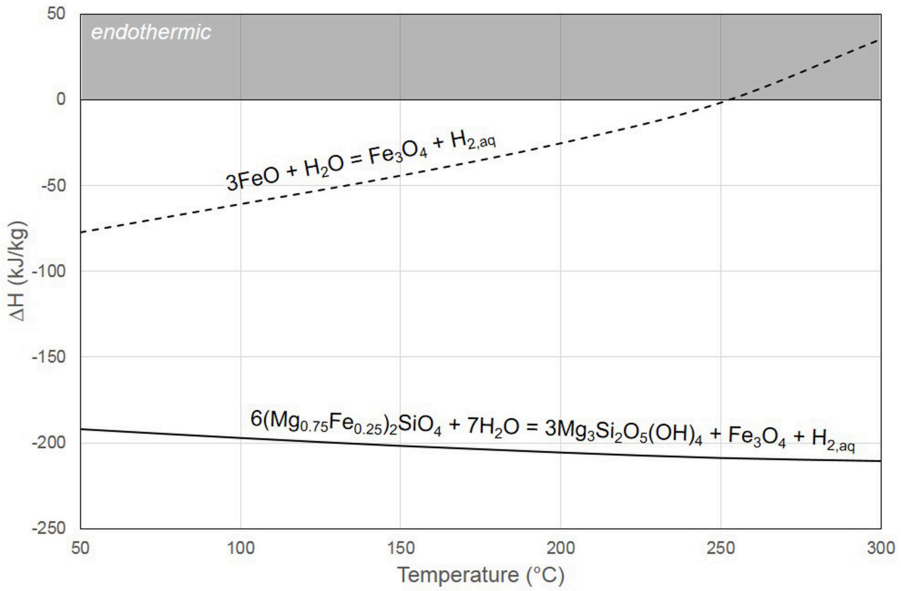

FIGURE 6 | Enthalpy of reaction in kJ per kg of starting material (including H_2O) at 20 MPa as a function of temperature. Whereas, serpentinization is strongly exothermic in the considered temperature range, wüstite oxidation in the presence of water becomes endothermic above 250°C.

exothermic contribution may arise from the hydration of calcium oxide into portlandite.

Experiments performed on FeO and olivine hydrothermal alteration revealed a major change in the reaction process marked by a change in kinetics behavior. In the case of FeO, this kinetics change occurs for a magnetite production rate of 1 $g_{Fe3O4}.L^{-1}.h^{-1}$ (150°C, 0.05 M), when magnetite precipitation becomes the rate limiting-step. Malvoisin et al. (2012a) observed a change in serpentinization kinetics at 300°C/50 MPa when decreasing olivine grain size down to 1–5 μm. The corresponding maximum magnetite precipitation rate, i.e., assuming that all iron from San Carlos olivine is transferred into the magnetite product, is estimated to be 0.25–0.3 $g_{Fe3O4}.L^{-1}.h^{-1}$. This rate is by three to four times lower than the rate at which magnetite precipitation (or Fe^{2+},aq oxidation associated to water splitting) becomes the rate-determining step as deduced by Crouzet et al. (2017a) from FeO oxidation experiments at 150°C. Therefore, the change in reaction process observed by Malvoisin et al. (2012a) is unlikely due to magnetite precipitation (or Fe^{2+},aq oxidation) becoming the rate-determining factor. The assumption by Malvoisin et al. (2012a) that the precipitation of the serpentine mineral (here chrysotile) is the rate-limiting step in this experiment is most likely.

Given the fact that olivine (or dunite) and BOF steel slag have similar HPC, one can wonder which of the two starting materials is the best suited for the fastest production of hydrogen and magnetite in the presence of initially pure water. The two rate-limiting processes are olivine and FeO (or magnesio-wüstite) dissolution which will occur, respectively, at near-neutral and alkaline pH due to the presence of Ca-oxide/hydroxide in the BOF steel slag. FeO dissolution data at alkaline pH are not available in the literature. In a first approach, one can use the data from Malvoisin et al. (2013), who obtained 50% reaction at 250°C after 1,400 h using a grinded BOF slag. A reaction rate of ca. 30–35% would be expected with the same unground slag (Brunet et al., 2014). SC olivine with grain sizes in the 5–15 μm range or below is needed to achieve a similar reaction rate. Therefore, unless additives are added (Andreani et al., 2013), intensive grinding is mandatory if using olivine-rich igneous rocks, since they usually contain olivine with grain sizes in the millimeter range. Reaction-induced olivine grain fracturing is no longer efficient for such small grain sizes (Malvoisin et al., 2017) and cannot therefore be considered to boost the reaction kinetics. From the available data, BOF steel slag appears therefore as a better suited candidate for H_2 and magnetite industrial production as far as reaction kinetics is concerned.

The Geo-Inspiration Value

Around 0.1–0.3 Mt H_2/year of H_2 are vented at mid-oceanic ridges (Cannat et al., 2010; Charlou et al., 2010; Keir, 2010), which cannot be reasonably recovered for human use. However, the natural redox processes that are involved in H_2 production can be simulated in the laboratory. The steam-iron process, which uses similar iron-oxidation reactions in the presence of vapor, was operated to produce H_2 before the counterpart geochemical process was discovered. Abiogenic H_2 production and its laboratory simulation led the geochemistry community to produce H_2 under hydrothermal conditions. This has been a source of inspiration to apply hydrothermal conditions to the treatment of BOF steel slags. Between 150 and 200 kg of steel slag is produced per ton of crude steel (Chand et al.,

2016). According to public data from the Worldsteel association, world production of crude steel reached around 1.8 billion tons in 2014. Consequently, around 250 million tons of steel slags were produced worldwide that year. The level of utilization of steel slags is highly variable from one country to another. According to Euroslag (www.euroslag.com), more than 75% of the steel slag that is produced in Europe is readily utilized, with road construction as main use. The situation is different in China or India, where utilization levels are closer to 25% (Yi et al., 2012; Chand et al., 2016). Based on the annual steel slag production, Malvoisin et al. (2013) evaluated that about 0.08 Mt/y of high-purity H_2 could be obtained (corresponding to 9 Mt/y of magnetite equivalent). This figure is only two or three times less than the amount of H_2 vented yearly at mid-oceanic ridges. One should, however, keep in mind that the amount of H_2 that could be obtained using the entire amount BOF slags produced yearly as well as the total amount of oceanic hydrogen that is emitted each year only represents a small amount compared to the H_2 that is consumed yearly by human activities (60 Mt H_2/y, Brown, 2016).

The major outcome of the geo-inspired treatment of steel slags is the formation of micro- to nanoparticles of magnetite, which was not anticipated and which directly arose from the use of hydrothermal conditions. The high value of magnetite in this size range opens new avenues to the valorization of ferrous iron-rich byproducts and wastes. Industrial magnetite manufactured for pigment application using the Laux method is sold for a few euros per kilogram; magnetite specifically manufactured for high-tech applications is expected to be sold at a higher price. The exact price, however, cannot be evaluated since a large-scale nanomagnetite market for high-tech applications (e.g., water depollution) is not yet in place. It can be conjectured that one kilogram of H_2 and one kilogram of nanomagnetite for high-tech applications will have similar prices (around 10 €/kg). It can thus be calculated from Reaction 4 that Fe-bearing waste recycling will produce 100 times more magnetite in weight than H_2. Therefore, the economic value of the hydrothermal process is clearly held by the magnetite product. The optimization of the magnetite process must stimulate new research with respect to hydrothermal iron oxidation which will have, in turn, applications to natural processes where very similar redox reactions do indeed occur. Several open questions remain to be addressed, such as the kinetics of water splitting and the role of impurities on magnetite (and H_2) production kinetics. The size of the recovered magnetite after steel slag hydrothermal treatment serves as a prompt for the investigation of the crystallization and growth of magnetite at the early stages of serpentinization. The determination of growth-rate laws for magnetite in the 150–300°C range at various pH would clearly have implications for both industrial and natural processes. The value of geo-inspired research can be seen as an opportunity to link applied and basic geochemical research with potential benefits for the two areas. The link is made possible by sharing investigation and modeling tools. Here, the same experimental and characterization tools have been used to study serpentinization and the hydrothermal treatment of steel slags. Geochemical tools have been used to identify the role of the main parameters on magnetite yield, namely temperature, pH and water-to-solid mass ratio. This type of modeling can be used as a support to optimize the conditions of possible industrial processes.

AUTHOR CONTRIBUTIONS

The author confirms being the sole contributor of this work and has approved it for publication.

ACKNOWLEDGMENTS

This review strongly benefitted from discussions with Benjamin Malvoisin, Camille Crouzet, Bruno Goffé, Laurence Raineau-Facchini, Nadir Recham, Isabelle Martinez, Vincent Milesi, and Céline Bonnaud. The CNRS Mission Interdisciplinaire is thanked for funding the GEO-INSPIRE interdisciplinary project which has gathered scientists from five different CNRS departments. The two reviewers are thanked for constructive reviews which helped to structure the garbled parts of the initial version. Smooth editorial handling of the manuscript by Jean-Philippe Perrillat is acknowledged.

REFERENCES

Abrajano, T. A., Sturchio, N. C., Bohlke, J. K., Lyon, G. L., Poreda, R. J., and Stevens, C. M. (1988). Methane-hydrogen gas seeps, Zambales ophiolite, Philippines: deep or shallow origin? *Chem. Geol.* 71, 211–222. doi: 10.1016/0009-2541(88)90116-7

Abrajano, T. A., Sturchio, N. C., Kennedy, B. M., Lyon, G. L., Muehlenbachs, K., and Bohlke, J. K. (1990). Geochemistry of reduced gas related to serpentinization of the Zambales ophiolite, Philippines. *Appl. Geochem.* 5, 625–630. doi: 10.1016/0883-2927(90)90060-I

Allen, D. E., and Seyfried, W. E. (2003). Compositional controls on vent fluids from ultramafic-hosted hydrothermal systems at mid-ocean ridges: an experimental study at 400°C, 500 bars. *Geochim. Cosmochim. Acta* 67, 1531–1542. doi: 10.1016/S0016-7037(02)01173-0

Andreani, M., Daniel, I., and Pollet-Villard, M. (2013). Aluminum speeds up the hydrothermal alteration of olivine. *Am. Mineral.* 98, 1738–1744. doi: 10.2138/am.2013.4469

Andreani, M., Mével, C., Boullier, A.-M., and Escartín, J. (2007). Dynamic control on serpentine crystallization in veins: constraints on hydration processes in oceanic peridotites. *Geochem. Geophys. Geosyst.* 8:Q02012. doi: 10.1029/2006GC001373

Aresta, M., Dibenedetto, A., and Angelini, A. (2014). Catalysis for the Valorization of exhaust carbon: from CO_2 to chemicals, materials, and fuels. technological use of CO_2. *Chem. Rev.* 114, 1709–1742. doi: 10.1021/cr400275s

Azad, A. M., Kesavan, S., and Al-Batty, S. (2008). Redemption of microscale mill waste into commercial nanoscale asset. *Key Eng. Mater.* 380, 229–255. doi: 10.4028/www.scientific.net/KEM.380.229

Baker, M. B., and Beckett, J. R. (1999). The origin of abyssal peridotites: a reinterpretation of constraints based on primary bulk compositions. *Earth Planet. Sci. Lett.* 171, 49–61. doi: 10.1016/S0012-821X(99)00130-2

Baumgartner, J., Dey, A., Bomans, P. H. H., Le Coadou, C., Fratzl, P., Sommerdijk, N. A. J. M., et al. (2013). Nucleation and growth of magnetite from solution. *Nat. Mater.* 12, 310–314. doi: 10.1038/nmat3558

Berndt, M. E., Allen, D. E., and Seyfried, W. E. (1996). Reduction of CO_2 during serpentinization of olivine at 300°C and 500 bar. *Geology* 24:351. doi: 10.1130/0091-7613(1996)024<0351:ROCDSO>2.3.CO;2

Bhushan, B. (2009). Biomimetics: lessons from nature–an overview. *Philos. Trans. R. Soc. A* 367, 1445–1486. doi: 10.1098/rsta.2009.0011

Blaney, L. (2007). Magnetite (Fe_3O_4): properties, synthesis, and applications. *Lehigh Rev.* 15, 32–81.

Boschi, C., Dini, A., Früh-Green, G. L., and Kelley, D. S. (2008). Isotopic and element exchange during serpentinization and metasomatism at the Atlantis Massif (MAR 30°N): insights from B and Sr isotope data. *Geochim. Cosmochim. Acta* 72, 1801–1823. doi: 10.1016/j.gca.2008.01.013

Brown, D. (2016). *U. S. and World H2 Production* 2014. CryoGas International.

Brunet, F., and Chopin, C. (1995). Bearthite, $Ca_2Al(PO_4)_2OH$: stability, thermodynamic properties and phase relations. *Contr. Mineral. Petrol.* 121, 258–266. doi: 10.1007/BF02688241

Brunet, F., Malvoisin, B., Vidal, O., and Goffe, B. (2014). *Method for Producing High-Purity Hydrogen Gas.* Available online at: https://patents.google.com/patent/US20160039669/

Camblor, M. (2006). The synthetic zeolites as geoinspired materials. *Macla* 6, 19–22.

Cannat, M., Fontaine, F., and Escartín, J. (2010). "Serpentinization and associated hydrogen and methane fluxes at slow spreading ridges," in *Geophysical Monograph Series*, eds. P. A. Rona, C. W. Devey, J. Dyment, and B. J. Murton (Washington, DC: American Geophysical Union), 241–264. doi: 10.1029/2008GM000760

Cannat, M., Sauter, D., Mendel, V., Ruellan, E., Okino, K., Escartin, J., et al. (2006). Modes of seafloor generation at a melt-poor ultraslow-spreading ridge. *Geology* 34, 605–608. doi: 10.1130/G22486.1

Chand, S., Paul, B., and Kumar, M. (2016). Sustainable approaches for LD slag waste management in steel industries: a review. *Metallurgist* 60, 116–128. doi: 10.1007/s11015-016-0261-3

Charlou, J.-L., and Donval, J.-P. (1993). Hydrothermal methane venting between 12°N and 26°N along the Mid-Atlantic Ridge. *J. Geophys. Res.* 98, 9625–9642. doi: 10.1029/92JB02047

Charlou, J. L., Donval, J. P., Fouquet, Y., Jean-Baptiste, P., and Holm, N. (2002). Geochemistry of high H2 and CH4 vent fluids issuing from ultramafic rocks at the Rainbow hydrothermal field (36°14′N, MAR). *Chem. Geol.* 191, 345–359. doi: 10.1016/S0009-2541(02)00134-1

Charlou, J. L., Donval, J. P., Konn, C., Ondréas, H., Fouquet, Y., Jean-Baptiste, P., et al. (2010). "High production and fluxes of H2 and CH4 and evidence of abiotic hydrocarbon synthesis by serpentinization in ultramafic-hosted hydrothermal systems on the Mid-Atlantic Ridge," in *Geophysical Monograph Series*, eds. P. A. Rona, C. W. Devey, J. Dyment, and B. J. Murton (Washington, DC: American Geophysical Union), 265–296. doi: 10.1029/2008GM000752

Chaurand, P., Rose, J., Domas, J., and Bottero, J.-Y. (2006). Speciation of Cr and V within BOF steel slag reused in road constructions. *J. Geochem. Explorat.* 88, 10–14. doi: 10.1016/j.gexplo.2005.08.006

Corrans, I. J., and Angove, J. E. (1991). Ultra fine milling for the recovery of refractory gold. *Miner. Eng.* 4, 763–776. doi: 10.1016/0892-6875(91)90064-3

Coveney, R., Goebel, E., Zeller, E., Dreschhoff, G., and Angino, E. (1987). Serpentinization and the origin of hydrogen gas in kansas. *AAPG Bull. Am. Assoc. Petr. Geol.* 71, 39–48.

Crouzet, C., Brunet, F., Montes-Hernandez, G., Recham, N., Findling, N., Ferrasse, J.-H., et al. (2017c). Hydrothermal valorization of steel slags—part i: coupled H_2 production and CO_2 mineral sequestration. *Front. Energy Res.* 5:29. doi: 10.3389/fenrg.2017.00029

Crouzet, C., Brunet, F., Recham, N., Auzende, A.-L., Findling, N., Magnin, V., et al. (2017b). Hydrothermal steel slag valorization—Part II: Hydrogen and nano-magnetite production. *Front. Earth Sci.* 5:86. doi: 10.3389/feart.2017.00086

Crouzet, C., Brunet, F., Recham, N., Findling, N., Lanson, M., Guyot, F., et al. (2017a). Hydrogen production by hydrothermal oxidation of FeO under acidic conditions. *Int. J. Hydrogen Energy* 42, 795–806. doi: 10.1016/j.ijhydene.2016.10.019

Daou, T. J., Pourroy, G., Bégin-Colin, S., Grenèche, J. M., Ulhaq-Bouillet, C., Legaré, P., et al. (2006). Hydrothermal synthesis of monodisperse magnetite nanoparticles. *Chem. Mater.* 18, 4399–4404. doi: 10.1021/cm060805r

Day, R., Halgedahl, S., Steiner, M., Kobayashi, K., Furuta, T., Ishii, T., et al. (1979). Magnetic properties of basalts from DSDP Leg 49. *Initial Rep. Deep Sea Drill. Proj.* 49, 781–791.

Decitre, S., Deloule, E., Reisberg, L., James, R., Agrinier, P., and Mével, C. (2002). Behavior of Li and its isotopes during serpentinization of oceanic peridotites. *Geochem. Geophys. Geosyst.* 3, 1–20. doi: 10.1029/2001GC000178

Deville, E., and Prinzhofer, A. (2016). The origin of N_2-H_2-CH_4-rich natural gas seepages in ophiolitic context: a major and noble gases study of fluid seepages in New Caledonia. *Chem. Geol.* 440, 139–147. doi: 10.1016/j.chemgeo.2016.06.011

Dunlop, D. J. (1981). The rock magnetism of fine particles. *Phys. Earth Planet. Inter.* 26, 1–26. doi: 10.1016/0031-9201(81)90093-5

Evans, B. W. (2008). Control of the products of serpentinization by the Fe2+Mg−1 exchange potential of olivine and orthopyroxene. *J. Petrology* 49, 1873–1887. doi: 10.1093/petrology/egn050

Ewan, B. C. R., and Allen, R. W. K. (2005). A figure of merit assessment of the routes to hydrogen. *Int. J. Hydrogen Energy* 30, 809–819. doi: 10.1016/j.ijhydene.2005.02.003

Flores, G. E., Campbell, J. H., Kirshtein, J. D., Meneghin, J., Podar, M., Steinberg, J. I., et al. (2011), Microbial community structure of hydrothermal deposits from geochemically different vent fields along the Mid-Atlantic Ridge. *Environ. Microbiol.* 13, 2158–2171. doi: 10.1111/j.1462-2920.2011.02463.x

Fratzl, P., and Barth, F. G. (2009). Biomaterial systems for mechanosensing and actuation. *Nature* 462, 442–448. doi: 10.1038/nature08603

Fujii, M., Okino, K., Sato, H., Nakamura, K., Sato, T., and Yamazaki, T. (2016). Variation in magnetic properties of serpentinized peridotites exposed on the Yokoniwa Rise, Central Indian Ridge: insights into the role of magnetite in serpentinization: magnetism of abyssal umtramafic rocks. *Geochem. Geophys. Geosyst.* 17, 5024–5035. doi: 10.1002/2016GC006511

Godard, M., Luquot, L., Andreani, M., and Gouze, P. (2013). Incipient hydration of mantle lithosphere at ridges: a reactive-percolation experiment. *Earth Planet. Sci. Lett.* 371–372, 92–102. doi: 10.1016/j.epsl.2013.03.052

Grosu, Y., Faik, A., Ortega-Fernández, I., and D'Aguanno, B. (2017). Natural Magnetite for thermal energy storage: excellent thermophysical properties, reversible latent heat transition and controlled thermal conductivity. *Solar Energy Mater. Solar Cells* 161, 170–176. doi: 10.1016/j.solmat.2016.12.006

Hacker, V., Fankhauser, R., Faleschini, G., Fuchs, H., Friedrich, K., Muhr, M., et al. (2000). Hydrogen production by steam–iron process. *J. Power Sources* 86, 531–535. doi: 10.1016/S0378-7753(99)00458-9

Hänchen, M., Prigiobbe, V., Storti, G., Seward, T. M., and Mazzotti, M. (2006). Dissolution kinetics of fosteritic olivine at 90–150°C including effects of the presence of CO2. *Geochim. Cosmochim. Acta* 70, 4403–4416. doi: 10.1016/j.gca.2006.06.1560

Hellmann, R. (1994). The albite-water system: Part I. The kinetics of dissolution as a function of pH at 100, 200 and 300°C. *Geochim. Cosmochim. Acta* 58, 595–611. doi: 10.1016/0016-7037(94)90491-X

Huang, R., Song, M., Ding, X., Zhu, S., Zhan, W., and Sun, W. (2017). Influence of pyroxene and spinel on the kinetics of peridotite serpentinization: the rates of peridotite serpentinization. *J. Geophys. Res.* 122, 7111–7126. doi: 10.1002/2017JB014231

Iyer, K., Jamtveit, B., Mathiesen, J., Malthe-Sørenssen, A., and Feder, J. (2008). Reaction-assisted hierarchical fracturing during serpentinization. *Earth Planet. Sci. Lett.* 267, 503–516. doi: 10.1016/j.epsl.2007.11.060

Jamtveit, B., Putnis, C. V., and Malthe-Sørenssen, A. (2009). Reaction induced fracturing during replacement processes. *Contrib. Mineral. Petrol.* 157, 127–133. doi: 10.1007/s00410-008-0324-y

Janecky, D. R., and Seyfried, W. E. (1986). Hydrothermal serpentinization of peridotite within the oceanic crust: experimental investigations of mineralogy and major element chemistry. *Geochim. Cosmochim. Acta* 50, 1357–1378. doi: 10.1016/0016-7037(86)90311-X

Jang, J.-H., and Brantley, S. L. (2009). Investigation of Wüstite (FeO) dissolution: implications for reductive dissolution of ferric oxides. *Environ. Sci. Technol.* 43, 1086–1090. doi: 10.1021/es8010139

Johnson, J. W., Oelkers, E. H., and Helgeson, H. C. (1992). SUPCRT92: A software package for calculating the standard molal thermodynamic properties of minerals, gases, aqueous species, and reactions from 1 to 5000 bar and 0 to 1000°C. *Comput. Geosci.* 18, 899–947. doi: 10.1016/0098-3004(92)90029-Q

Juckes, L. M. (2003). The volume stability of modern steelmaking slags. *Mineral Process. Extract. Metall.* 112, 177–197. doi: 10.1179/037195503225003708

Keir, R. S. (2010). A note on the fluxes of abiogenic methane and hydrogen from mid-ocean ridges: abiogenic methane and hydrogen fluxes. *Geophys. Res. Lett.* 37. doi: 10.1029/2010GL045362

Kelemen, P. B., and Hirth, G. (2012). Reaction-driven cracking during retrograde metamorphism: olivine hydration and carbonation. *Earth Planet. Sci.Lett.* 345–348, 81–89. doi: 10.1016/j.epsl.2012.06.018

Kelley, D. S., Karson, J. A., Blackman, D. K., Früh-Green, G. L., Butterfield, D. A., Lilley, M. D., et al. (2001). An off-axis hydrothermal vent field near the Mid-Atlantic Ridge at 30°N. *Nature* 412, 145–149. doi: 10.1038/35084000

Kelley, D. S., Karson, J. A., Früh-Green, G. L., Yoerger, D. R., Shank, T. M., Butterfield, D. A., et al. (2005). A serpentinite-hosted ecosystem: the lost city hydrothermal field. *Science* 307, 1428–1434. doi: 10.1126/science.1102556

Klein, F., Bach, W., Humphris, S. E., Kahl, W.-A., Jöns, N., Moskowitz, B., et al. (2014). Magnetite in seafloor serpentinite—Some like it hot. *Geology* 42, 135–138. doi: 10.1130/G35068.1

Klein, F., Bach, W., Jöns, N., McCollom, T., Moskowitz, B., and Berquó, T. (2009). Iron partitioning and hydrogen generation during serpentinization of abyssal peridotites from 15°N on the Mid-Atlantic Ridge. *Geochim. Cosmochim. Acta* 73, 6868–6893. doi: 10.1016/j.gca.2009.08.021

Klein, F., Bach, W., and McCollom, T. M. (2013). Compositional controls on hydrogen generation during serpentinization of ultramafic rocks. *Lithos* 178, 55–69. doi: 10.1016/j.lithos.2013.03.008

Kularatne, K., Sissmann, O., Kohler, E., Chardin, M., Noirez, S., and Martinez, I. (2018). Simultaneous ex-situ CO2 mineral sequestration and hydrogen production from olivine-bearing mine tailings. *Appl. Geochem.* 95, 195–205. doi: 10.1016/j.apgeochem.2018.05.020

Lafay, R., Fernandez-Martinez, A., Montes-Hernandez, G., Auzende, A. L., and Poulain, A. (2016). Dissolution-reprecipitation and self-assembly of serpentine nanoparticles preceding chrysotile formation: insights into the structure of proto-serpentine. *Am. Mineral.* 101, 2666–2676. doi: 10.2138/am-2016-5772

Lafay, R., Montes-Hernandez, G., Janots, E., Chiriac, R., Findling, N., and Toche, F. (2012). Mineral replacement rate of olivine by chrysotile and brucite under high alkaline conditions. *J. Cryst. Growth* 347, 62–72. doi: 10.1016/j.jcrysgro.2012.02.040

Lasaga, A. C. (1984). Chemical kinetics of water-rock interactions. *J. Geophys. Res.* 89, 4009–4025. doi: 10.1029/JB089iB06p04009

Liu, L.-H., Tsai, Y.-C., and Chen, D.-H. (2016). Catalyst-enhanced hydrothermal generation of highly pure compressed hydrogen gas from iron micro-powders. *RSC Adv.* 6, 86938–86942. doi: 10.1039/C6RA19947J

Long, L. Q., Hue, T. T. B., Hoan, N. X., Cuong, L. V., Thang, P. D., Hoang, T., et al. (2016). Growth mechanism and stability of magnetite nanoparticles synthesized by the hydrothermal method. *J. Nanosci. Nanotechnol.* 16, 7373–7379. doi: 10.1166/jnn.2016.11110

Lorente, E., Peña, J. A., and Herguido, J. (2011). Cycle behaviour of iron ores in the steam-iron process. *Int. J. Hydrogen Energy* 36, 7043–7050. doi: 10.1016/j.ijhydene.2011.03.069

Maffione, M., Morris, A., Plümper, O., and van Hinsbergen, D. J. J. (2014). Magnetic properties of variably serpentinized peridotites and their implication for the evolution of oceanic core complexes. *Geochem. Geophys. Geosyst.* 15, 923–944. doi: 10.1002/2013GC004993

Malvoisin, B. (2015). Mass transfer in the oceanic lithosphere: serpentinization is not isochemical. *Earth Planet. Sci. Lett.* 430, 75–85. doi: 10.1016/j.epsl.2015.07.043

Malvoisin, B., Brantut, N., and Kaczmarek, M.-A. (2017). Control of serpentinisation rate by reaction-induced cracking. *Earth Planet. Sci. Lett.* 476, 143–152. doi: 10.1016/j.epsl.2017.07.042

Malvoisin, B., and Brunet, F. (2014). Water diffusion-transport in a synthetic dunite: consequences for oceanic peridotite serpentinization. *Earth Planet. Sci. Lett.* 403, 263–272. doi: 10.1016/j.epsl.2014.07.004

Malvoisin, B., Brunet, F., Carlut, J., Montes-Hernandez, G., Findling, N., Lanson, M., et al. (2013). High-purity hydrogen gas from the reaction between BOF steel slag and water in the 473–673 K range. *Int. J. Hydrogen Energy* 38, 7382–7393. doi: 10.1016/j.ijhydene.2013.03.163

Malvoisin, B., Brunet, F., Carlut, J., Rouméjon, S., and Cannat, M. (2012a). Serpentinization of oceanic peridotites: 2. Kinetics and processes of San Carlos olivine hydrothermal alteration. *J. Geophys. Res.* 117. doi: 10.1029/2011JB008842

Malvoisin, B., Carlut, J., and Brunet, F. (2012b). Serpentinization of oceanic peridotites: 1. A high-sensitivity method to monitor magnetite production in hydrothermal experiments. *J. Geophys. Res.* 117. doi: 10.1029/2011JB008612

Mao, B., Kang, Z., Wang, E., Lian, S., Gao, L., Tian, C., et al. (2006). Synthesis of magnetite octahedrons from iron powders through a mild hydrothermal method. *Mater. Res. Bull.* 41, 2226–2231. doi: 10.1016/j.materresbull.2006.04.037

Marcaillou, C., Muñoz, M., Vidal, O., Parra, T., and Harfouche, M. (2011). Mineralogical evidence for H2 degassing during serpentinization at 300°C/300 bar. *Earth Planet. Sci. Lett.* 303, 281–290. doi: 10.1016/j.epsl.2011.01.006

Martin, B., and Fyfe, W. S. (1970). Some experimental and theoretical observations on the kinetics of hydration reactions with particular reference to serpentinization. *Chem. Geol.* 6, 185–202. doi: 10.1016/0009-2541(70)90018-5

Matsuura, H., and Tsukihashi, F. (2012). Thermodynamic calculation of generation of H2 gas by reaction between FeO in Steelmaking slag and water vapor. *ISIJ Int.* 52, 1503–1512. doi: 10.2355/isijinternational.52.1503

Mayhew, L. E., Ellison, E. T., McCollom, T. M., Trainor, T. P., and Templeton, A. S. (2013). Hydrogen generation from low-temperature water–rock reactions. *Nat. Geosci.* 6, 478–484. doi: 10.1038/ngeo1825

McCollom, T. M., and Bach, W. (2009). Thermodynamic constraints on hydrogen generation during serpentinization of ultramafic rocks. *Geochim. Cosmochim. Acta* 73, 856–875. doi: 10.1016/j.gca.2008.10.032

McCollom, T. M., Klein, F., Robbins, M., Moskowitz, B., Berqu,ó, T. S., Jöns, N., et al. (2016). Temperature trends for reaction rates, hydrogen generation, and partitioning of iron during experimental serpentinization of olivine. *Geochim. Cosmochim. Acta* 181, 175–200. doi: 10.1016/j.gca.2016.03.002

McColm, I. J. (2013). *Dictionary of Ceramic Science and Engineering.* Dordrecht: Springer. Available online at: http://link.springer.com/10.1007/978-94-007-0916-4 (Accessed October 14, 2016).

Michiels, K., Haesen, A., Meynen, V., and Spooren, J. (2018). Applicability of fine industrial metallic iron-rich waste powders for hydrothermal production of hydrogen gas: the influence of non-ferrous contaminants. *J. Clean. Prod.* 195, 674–686. doi: 10.1016/j.jclepro.2018.05.251

Michiels, K., Spooren, J., and Meynen, V. (2015). Production of hydrogen gas from water by the oxidation of metallic iron under mild hydrothermal conditions, assisted by *in situ* formed carbonate ions. *Fuel* 160, 205–216. doi: 10.1016/j.fuel.2015.07.061

Mombelli, D., Mapelli, C., Barella, S., Di Cecca, C., Le Saout, G., and Garcia-Diaz, E. (2016). The effect of microstructure on the leaching behaviour of electric arc furnace (EAF) carbon steel slag. *Process Saf. Environ. Protect.* 102, 810–821. doi: 10.1016/j.psep.2016.05.027

Moody, J. B. (1976). Serpentinization: a review. *Lithos* 9, 125–138. doi: 10.1016/0024-4937(76)90030-X

Murugan, A., Thursfield, A., and Metcalfe, I. S. (2011). A chemical looping process for hydrogen production using iron-containing perovskites. *Energy Environ. Sci.* 4, 4639–4649. doi: 10.1039/C1EE02142G

Neal, C., and Stanger, G. (1983). Hydrogen generation from mantle source rocks in Oman. *Earth Planet. Sci. Lett.* 66, 315–320. doi: 10.1016/0012-821X(83)90144-9

Niu, Y. (2004). Bulk-rock major and trace element compositions of abyssal peridotites: implications for mantle melting, melt extraction and post-melting processes beneath mid-ocean ridges. *J Petrology* 45, 2423–2458. doi: 10.1093/petrology/egh068

Normand, C., Williams-Jones, A. E., Martin, R. F., and Vali, H. (2002). Hydrothermal alteration of olivine in a flow-through autoclave: nucleation and growth of serpentine phases. *Am. Mineral.* 87, 1699–1709. doi: 10.2138/am-2002-11-1220

Okada, K., Isobe, T., Katsumata, K., Kameshima, Y., Nakajima, A., and MacKenzie, K. J. D. (2011). Porous ceramics mimicking nature—preparation and properties of microstructures with unidirectionally oriented pores. *Sci. Technol. Adv. Mater.* 12:064701. doi: 10.1088/1468-6996/12/6/064701

Okamoto, A., Ogasawara, Y., Ogawa, Y., and Tsuchiya, N. (2011). Progress of hydration reactions in olivine–H2O and orthopyroxenite–H2O systems at 250°C and vapor-saturated pressure. *Chem. Geol.* 289, 245–255. doi: 10.1016/j.chemgeo.2011.08.007

Oufi, O., Cannat, M., and Horen, H. (2002). Magnetic properties of variably serpentinized abyssal peridotites. *J. Geophys. Res.* 107, EPM 3-1-EPM 3-19. doi: 10.1029/2001JB000549

Page, N. J. (1968). Chemical differences among the serpentine "polymorphs." *American Mineralogist* 53, 201–215.

Palandri, J. L., and Kharaka, Y. K. (2004). *A Compilation of Rate Parameters of Water-Mineral Interaction Kinetics for Application to Geochemical Modeling.* Menlo Park, CA: Geological Survey. Available online at: http://www.dtic.mil/docs/citations/ADA440035 (Accessed October 22, 2018).

Pens, M., Andreani, M., Daniel, I., Perrillat, J.-P., and Cardon, H. (2016). Contrasted effect of aluminum on the serpentinization rate of olivine and orthopyroxene under hydrothermal conditions. *Chem. Geol.* 441, 256–264. doi: 10.1016/j.chemgeo.2016.08.007

Plümper, O., Røyne, A., Magras,ó, A., and Jamtveit, B. (2012). The interface-scale mechanism of reaction-induced fracturing during serpentinization. *Geology* 40, 1103–1106. doi: 10.1130/G33390.1

Pokrovsky, O. S., and Schott, J. (2000). Kinetics and mechanism of forsterite dissolution at 25°C and pH from 1 to 12. *Geochim. Cosmochim. Acta* 64, 3313–3325. doi: 10.1016/S0016-7037(00)00434-8

Regazzoni, A. E., Urrutia, G. A., Blesa, M. A., and Maroto, A. J. G. (1981). Some observations on the composition and morphology of synthetic magnetites obtained by different routes. *J. Inorg. Nuclear Chem.* 43, 1489–1493. doi: 10.1016/0022-1902(81)80322-3

Rouméjon, S., and Cannat, M. (2014). Serpentinization of mantle-derived peridotites at mid-ocean ridges: mesh texture development in the context of tectonic exhumation. *Geochem. Geophys. Geosyst.* 15, 2354–2379. doi: 10.1002/2013GC005148

Rudge, J. F., Kelemen, P. B., and Spiegelman, M. (2010). A simple model of reaction-induced cracking applied to serpentinization and carbonation of peridotite. *Earth Planet. Sci. Lett.* 291, 215–227. doi: 10.1016/j.epsl.2010.01.016

Ruiz-Agudo, E., Putnis, C. V., and Putnis, A. (2014). Coupled dissolution and precipitation at mineral–fluid interfaces. *Chem. Geol.* 383, 132–146. doi: 10.1016/j.chemgeo.2014.06.007

Sano, Y., Urabe, A., Wakita, H., and Wushiki, H. (1993). Origin of hydrogen-nitrogen gas seeps, Oman. *Appl. Geochem.* 8, 1–8. doi: 10.1016/0883-2927(93)90053-J

Shatokha, V., Sokur, I., and Kamkina, L. (2016). Study on water splitting potential of some metallurgical wastes for production of hydrogen. *J. Sustain. Metall.* 2, 116–122. doi: 10.1007/s40831-015-0038-0

Shimizu, H., and Okamoto, A. (2016). The roles of fluid transport and surface reaction in reaction-induced fracturing, with implications for the development of mesh textures in serpentinites. *Contrib. Mineral. Petrol.* 171:73. doi: 10.1007/s00410-016-1288-y

Ter Teo, P., Seman, A. A., Basu, P., and Sharif, N. M. (2016). Characterization of EAF Steel slag waste: the potential green resource for ceramic tile production. *Procedia Chem.* 19, 842–846. doi: 10.1016/j.proche.2016.03.111

Thayer, T. P. (1966). Serpentinization considered as a constant-volume metasomatic process. *Am. Mineral.* 51, 685–710.

Vayssières, L., Chanéac, C., Tronc, E., and Jolivet, J. P. (1998). Size tailoring of magnetite particles formed by aqueous precipitation: an example of thermodynamic stability of nanometric oxide particles. *J. Colloid Interface Sci.* 205, 205–212. doi: 10.1006/jcis.1998.5614

Vils, F., Tonarini, S., Kalt, A., and Seitz, H.-M. (2009). Boron, lithium and strontium isotopes as tracers of seawater–serpentinite interaction at Mid-Atlantic ridge, ODP Leg 209. *Earth Planet. Sci. Lett.* 286, 414–425. doi: 10.1016/j.epsl.2009.07.005

Vincent, J. F. V., Bogatyreva, O. A., Bogatyrev, N. R., Bowyer, A., and Pahl, A.-K. (2006). Biomimetics: its practice and theory. *J. R. Soc. Interface* 3, 471–482. doi: 10.1098/rsif.2006.0127

Wang, Q., and Yan, P. (2010). Hydration properties of basic oxygen furnace steel slag. *Construct. Build. Mater.*24, 1134–1140. doi: 10.1016/j.conbuildmat.2009.12.028

Wegner, W. W., and Ernst, W. G. (1983). Experimentally determined hydration and dehydration reaction rates in the system MgO-SiO2-H2O. *Am. J. Sci.* 283-A, 151–180.

Welhan, J. A., and Craig, H. (1979). Methane and hydrogen in East Pacific Rise hydrothermal fluids. *Geophys. Res. Lett.* 6, 829–831. doi: 10.1029/GL006i011p00829

Wetzel, L. R., and Shock, E. L. (2000). Distinguishing ultramafic-from basalt-hosted submarine hydrothermal systems by comparing calculated vent fluid compositions. *J. Geophys. Res.* 105, 8319–8340. doi: 10.1029/1999JB900382

Williams, L. O. (1980). *Hydrogen Power: An Introduction to Hydrogen Energy and Its Applications*. Oxford: Pergamon Press, 168.

Wogelius, R. A., and Walther, J. V. (1991). Olivine dissolution at 25°C: effects of pH, CO2, and organic acids. *Geochim. Cosmochim. Acta* 55, 943–954. doi: 10.1016/0016-7037(91)90153-V

Yi, H., Xu, G., Cheng, H., Wang, J., Wan, Y., and Chen, H. (2012). An overview of utilization of steel slag. *Proced. Environ. Sci.* 16, 791–801. doi: 10.1016/j.proenv.2012.10.108

Yildirim, I. Z., and Prezzi, M. (2011). Chemical, mineralogical, and morphological properties of steel slag. *Adv. Civil Eng.* 2011:e463638. doi: 10.1155/2011/463638

Zgonnik, V., Beaumont, V., Deville, E., Larin, N., Pillot, D., and Farrell, K. M. (2015). Evidence for natural molecular hydrogen seepage associated with Carolina bays (surficial, ovoid depressions on the Atlantic Coastal Plain, Province of the USA). *Progress Earth Planet. Sci.* 2:31. doi: 10.1186/s40645-015-0062-5

Conflict of Interest Statement: The author declares that the research was conducted in the absence of any commercial or financial relationships that could be construed as a potential conflict of interest.